Ionics (2024) 30:61–84
https://doi.org/10.1007/s11581-023-05269-4

REVIEW

Recent developments in noble metal–based hybrid electrocatalysts for overall water splitting

Anandajayarajan Udayakumar[1] · Preethi Dhandapani[1] · Senthilkumar Ramasamy[2] · Chao Yan[3] · Subramania Angaiah[1]

Received: 30 August 2023 / Revised: 3 October 2023 / Accepted: 17 October 2023 / Published online: 1 November 2023

Abstract

The quest for sustainable energy sources has accelerated the exploration of water splitting as a method of clean hydrogen production. Among the various electrocatalysts designed to drive water splitting, noble metal–based electrocatalysts have recently emerged as promising candidates. This review highlights the recent developments in noble metal–based electrocatalysts for overall water splitting. These electrocatalysts integrate the exceptional catalytic properties of noble metals, such as platinum, iridium, and ruthenium, with diverse materials, including transition metals, carbon substrates, and metal oxides, to enhance their efficiency, stability, and cost-effectiveness. This review discusses recent developments on noble metals such as platinum, palladium, rhodium, ruthenium, iridium, and noble metal–based hybrid materials as bifunctional electrocatalysts for overall water splitting. In addition, the existing obstacles and prospects for bifunctional water-splitting electrocatalysts are also focused.

Keywords Hydrogen production · Noble metal · Electrocatalyst · Energy conversion · Water splitting

Introduction

The ever-increasing use of fossil fuels generates a series of catastrophes, including air pollution, energy shortages, and climate change, enabling swift progress in renewable, environmentally friendly alternative energy sources [1–5]. In the context of pollution issues, finding clean, cost-effective, and renewable energy resources seems to be a critical objective for achieving long-term growth [6–8]. In such a case, hydrogen remains a viable alternative to traditional fossil fuels since it is a sustainable, more efficient, and flexible energy source. H_2 is an outstanding energy transporter and a strong applicant for prospective low-carbon energy systems because of its very high gravitational energy density and combustion by-product that remains environment-friendly, especially with water [9–11]. Furthermore, hydrogen is the most plentiful element in the cosmos and is mostly stored in the world's vast water resources. As a result, water decomposition serves as a better approach for hydrogen production due to its sustainability and environmental friendliness [12, 13]. The water-splitting process can be accomplished using electricity or light. Electrocatalytic water splitting is a more practical technology than photocatalytic water splitting because it has a better conversion efficiency and higher hydrogen generation purity [14–17]. In general, water splitting demands significantly greater voltage than the theoretical voltage (1.23 V) due to the slow kinetics of the oxygen evolution reaction (OER) and hydrogen evolution reaction (HER) of water electrolysis [18, 19]. As a result, developing high-efficiency catalysts for decreasing the overpotential associated with the cathodic HER and anodic OER is critical for accelerating H_2 and O_2 generation [20–22]. Despite significant efforts toward hydrogen production, noble metal and its alloy continue to be the efficient and effective electrocatalyst. To date, noble metal–based catalysts and their derivatives have proven to

✉ Subramania Angaiah
a.subramania@gmail.com

[1] Electro-Materials Research Laboratory, Centre for Nanoscience and Technology, Pondicherry University, Puducherry 605014, India

[2] Department of Chemical Engineering and Materials Science, Amrita Vishwa Vidyapeetham, Coimbatore 641112, India

[3] School of Materials Science and Engineering, Jiangsu University of Science and Technology, Zhenjiang 212003, PR China

be effective electrocatalysts for HER, whereas OER electrocatalysts rely on iridium and ruthenium at the industrial level [23–26]. However, noble metals' high price and scarcity tend to restrict their application in industries. As an outcome, scientists have devised several solutions to these issues, including shrinking noble metals to single atoms anchored on a porous conductive carbon-based matrix by hybridizing and alloying them with less expensive transition metals. Additionally, interface engineering is also used to solve their high price and instability [27, 28].

In the past few decades, many advanced noble metal–based electrocatalysts have been successfully developed for boosting water splitting, and some reviews regarding the electrocatalytic performance studies of noble metal catalysts have been published. However, the advances in noble metals and their derivatives as electrocatalysts for accelerating water splitting have not been systematically summarized. Considering the significant potential of water electrolysis and the great merits of noble metals and their derivatives as electrocatalysts, a comprehensive review should be made. Herein, we summarized the recent progress toward noble metals and their derivatives in the field of electrocatalytic water splitting with a particular emphasis on the merits of nanostructures. Moreover, some representative noble metal–based electrocatalysts and many effective strategies for optimizing their electrocatalytic performance have also been manifested. Lastly, the challenging issues and future directions of noble metal–based electrocatalysts in electrochemical water splitting are also outlined.

Electrochemistry of overall water-splitting reaction

The overall water splitting is a very straightforward chemical reaction: $2H_2O \rightarrow 2H_2 + O_2$. It primarily consists of two half-reactions that practically co-occur: the cathodic hydrogen evolution reaction and the anodic oxygen evolution reaction, which necessitates the four-electron transfer. However, the overall water-splitting reaction varies depending on the pH of the solution. Along with pH, the electrolyte involved also plays a major role. According to the Nernst equation, acidic environments encourage HER, while OER proceeds more easily in alkaline environments. Figure 1 shows the schematic representation of a conventional water electrolyzer [29].

In alkaline medium:		
At anode:	$4OH^- \rightarrow 2H_2O + O_2 + 4e^-$	$E^\circ = -0.40$ V
At cathode:	$4H_2O + 2e^- \rightarrow 2H_2 + 4OH^-$	$E^\circ = -0.83$ V
In acidic medium:		
At anode:	$2H_2O \rightarrow O_2 + 4H^+ + 4e^-$	$E^\circ = -1.23$ V
At cathode:	$4H^+ + e^- \rightarrow H_2$	$E^\circ = 0$ V

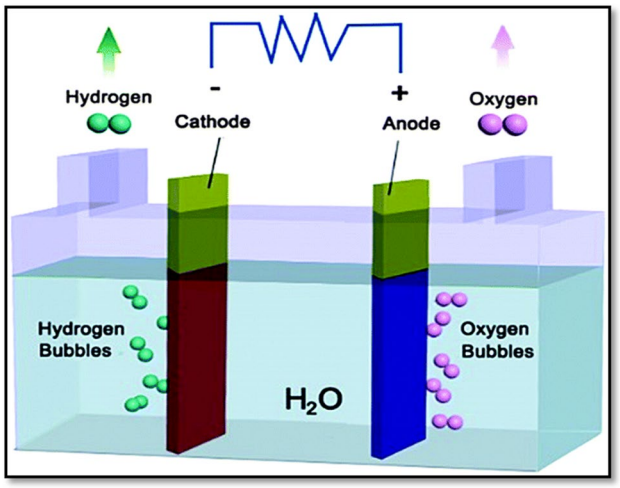

Fig. 1 Schematic representation of conventional water electrolyzer [29] reproduced with permission from ref. 27, copyright 2020, International Journal of Hydrogen Energy

Hydrogen evolution reaction (HER)

The HER process is a two-electron reaction that starts with the adsorption of water molecules at catalytic active sites (Volmer step) and ends with the successive desorption of water molecules from the surface of the electrocatalyst through either electrochemical desorption (Heyrovsky step) or chemical desorption (Tafel recombination). Therefore, the generic response path could be represented by either the Volmer-Heyrovsky or Volmer-Tafel path.

Mechanism of HER catalysis in alkaline medium

Step I:
Volmer reaction: $H_2O + e^- \rightarrow OHv^- + H_{ads}$
Step II:
Heyrovsky step: $H_2O + H_{ads} + e^- \rightarrow OHv^- + H_2$
Step III:
Tafel reaction: $2H_{ads} \rightarrow H_2$

Mechanism of HER catalysis in acidic medium

Step I:
Volmer reaction: $H^+ + e^- \rightarrow H_{ads}$
Step II:
Heyrovsky step: $H_{ads} + H^+ + e^- \rightarrow H_2$
Step III:
Tafel reaction: $H_{ads} + H_{ads} \rightarrow H_2$

Oxygen evolution reaction (OER)

As the OER process comprises complex routes with multi-stage four-electron transfer, particularly with slower kinetics, the OER process is significantly more difficult than the HER.

Mechanism of OER catalysis in acidic medium

The total oxidation process of water is

$$2H_2O_{(l)} \rightarrow O_2 + 4H^+ + 4e^-; \Delta G_0 = 4.92\text{eV}$$

The underlying mechanisms for a typical catalytic surface are as follows [30]:

$$M + H_2O_{(l)} \rightarrow M - OH + H^+ + e^-$$

$$M - OH + OH^- \rightarrow M - O + H_2O_{(l)} + e^-$$

$$M - O \rightarrow 2M + O_{2(g)}$$

$$M - O + H_2O_{(l)} \rightarrow M - OOH + H^+ + e^-$$

$$M - OOH + H_2O_{(l)} \rightarrow M + O_{2(g)} + H^+ + e^-$$

Mechanism of OER catalysis in alkaline medium

The overall reaction is as follows [29–31]:

$$4OH^-_{(aq)} \rightarrow 2H_2O_{(aq)} + 4e^- + O_{2\,(g)}$$

The OER follows the multi-step process below [31]:

$$M + OH^- \rightarrow M\text{–}OH$$

$$M - OH + OH^- \rightarrow M - O + H_2O(l)$$

$$2M\text{–}O \rightarrow 2M + O_2(g)$$

$$M\text{–}O + OH^- \rightarrow M\text{–}OOH + e^-$$

$$M - OOH + OH^- \rightarrow M + O_2(g) + H_2O(l)$$

Parameters for the evaluation of electrocatalytic performance

Though several factors must be considered to assess an electrocatalyst for water splitting, they can be grouped under three main categories: activity, stability, and efficiency. Furthermore, the activity is influenced by several variables, including overpotential, Tafel slope, and exchange current density, which can be deduced from polarization curves. The stability is described by the overpotential or current change over time. On the other hand, the efficiency comprises the Faradaic efficiency and the turnover frequency (TOF).

Electrocatalytic activity

Overpotential

Overpotential (η) is a crucial criterion for assessing electrocatalyst performance. At standard conditions of 25 °C and 1 atm, the potential required for water splitting is 1.23 V [32]. Nonetheless, this potential (1.23 V) is more than the stated value. This unanticipated reaction is so ubiquitous in electrochemistry that is known as overpotential. As a result, the applied potential must be raised for an electrolytic reaction to occur.

The overpotential is given by the formula:

$$\eta = E_{\text{Applied}} - E_0 - iR$$

where iR is the ohmic correction, E_0 is the theoretical equilibrium value, and E_{applied} is applied potential. In short, overpotential (η) is largely utilized to overpower the intrinsic activation barriers existing on the anode (η_a) and cathode (η_c) and a variety of additional resistances (η_{other}), such as solution and contact resistances [32]. For example, N-doped carbon-wrapped Ir-doped Ni nanoparticle composites supported on Ni foam exhibit low overpotentials of 32 mV at 10 mA cm^{-2} for HER, while it exhibits an overpotential of 329 mV at 50 mA cm^{-2} for OER [33]. Similarly, SrIrO developed by L. Zhang et al. displays an extremely low overpotential of 245 mV for OER and 18.2 mV for HER at 10 mA cm^{-2} [34]. In summary, a good catalyst should attain a greater current density while having a smaller overpotential [35].

Tafel slope and exchange current density

The Tafel slope (b) and the exchange current density (j_0) utilized to assess the electrocatalyst activity are calculated using the Tafel equation [30, 36, 37]:

$$\eta = a + blog(|j|)$$

$$\left(a = 2.303RT\ \log\left(j_0\right)/\alpha nF, b = 2.303RT/\alpha nF\right)$$

where η is the overpotential which is the variation in potential of the electrode and standard potentials ($\eta = E - E_0$), b is the Tafel slope value, j is the measured current density, j_0 is the exchange current density, T is the

temperature, R is the gas constant, n is the number of transferred electrons in the electrochemical redox reaction, F is the Faraday constant (96,485 C mol^{-1}), and α is the charge transfer coefficient. In addition, the exchange current density (j_0) is the overpotential value when the current density is zero, indicating the electrochemical process rate [30, 37]. For example, S. Zhang et al. reported the synthesis of nickel (Ni)-iridium (Ir) alloy nanoparticles/graphene hybrids for overall water splitting. As a result, the Tafel slope of $Ni_{0.93}Ir_{0.07}$/rGO (64.3 mV dec^{-1}) is found to be smaller than that of Ir/rGO (118.7 mV dec^{-1}) and Ir/C (74.3 mV dec^{-1}) [38]. Therefore, the electrocatalyst with a lower Tafel slope (b) and higher exchange current density (j_0) seem to be the desirable characteristics for water splitting.

Electrocatalytic efficiency

Faradaic efficiency

Faradic efficiency is an important measure that reflects the efficiency of electron usage during the electrochemical process. It is defined as the ratio of the experimentally discovered amount of H_2 or O_2 to the theoretically estimated amount of H_2 or O_2. Because of the rare side reaction, water splitting has a high Faradic efficiency, which benefits practical applications for energy usage efficiency [32]. For example, NiFe-LDH nanosheets developed by H. Sun et al. exhibited a faradaic efficiency of ~ 100% demonstrating that all the electrons are involved in catalytic reactions [39].

Turnover frequency (TOF)

The term TOF describes the amount of reactant a catalyst can transform into the desired product per catalytic site in a given amount of time [40]. The TOF is calculated by the formula:

$$TOF = JA/\alpha Fn$$

where j represents current density and A represents the working electrode's surface area. α indicate the electron number (electrons/mol) of the target product. F is Faraday's constant (96,485.3 C mol^{-1}), and the number n denotes the number of moles of active materials determined by calculating electrochemically active surface area (ECSA). Furthermore, not all atoms are catalytically active and equally accessible. As a result, obtaining an exact TOF value is challenging.

Bifunctional electrocatalysts

Electrochemical water splitting is recognized as a viable method for producing hydrogen, which can be used to replace fossil fuels and store energy sustainably. Developing highly efficient and low-cost electrocatalysts is vital to the large-scale implementation of hydrogen energy devices. Bifunctional electrocatalysts that work for both HER and OER are favorable for the overall water-splitting systems, promoting the system's performance and simplifying the system design. In recent years, noble metal–based compounds have been extensively explored and employed as bifunctional electrocatalysts for overall water splitting, such as platinum, palladium, ruthenium, iridium, inter-noble metals, and hybrids.

Noble metal–based electrocatalysts for water splitting

Initially, non-precious metals and non-metal-based electrocatalysts have garnered significant interest in the field of electrochemistry due to their potential that reduce costs and alleviate the reliance on scarce and expensive precious metals like platinum and palladium. However, they also come with some drawbacks, which can limit their widespread adoption in various electrochemical applications. Here are some of the disadvantages associated with non-precious metals and non-metal-based electrocatalysts such as lower catalytic activity and limited selectivity and stability. Non-precious metal electrocatalysts often exhibit lower catalytic activity than their precious metal counterparts, which means they may require higher overpotentials (applied voltage exceeding the thermodynamic minimum) to drive electrochemical reactions effectively, which can result in lower energy efficiency. In addition, they are susceptible to degradation over time, especially under harsh electrochemical conditions, reducing their long-term stability and performance.

The best and most practical materials in terms of performance for electrocatalytic water splitting are the noble metal–based compounds such as platinum (Pt), palladium (Pd), rhodium (Rh), ruthenium (Ru), and iridium (Ir), collectively called the "platinum-group metal" (PGM). To date, Pt/C is set as a benchmark for comparing the performance of upcoming electrocatalysts and is commercially used worldwide in essential places. Nevertheless, its limited storage capacity, availability, and high price hinder the commercialization of noble metal–based catalysts. To meet this problem, sensible catalyst designs with minimal metal loading and high metal utilization are required.

Platinum (Pt)-based materials

Platinum (Pt) and Pt-based alloys are currently regarded as state-of-the-art for HER catalytic materials, owing to the beneficial development of $Pt–H_{ads}$ at the active sites, which allows for adequate water molecule adsorption. However, the

high cost, limited elemental sources, and inferior durability of Pt-based catalysts have severely hampered their wide usage. Thus, using a bifunctional electrocatalyst simplifies the water-splitting process, reduces costs, and enhances the overall electrocatalytic efficiency. However, poor OER performance of platinum has hampered the development of perfect water-splitting systems. Though Pt serves as a benchmark for HER catalyst, the catalytic activity of Pt is hampered by water dissociation due to an insufficient oxyphilic surface to divide the O–H bond of water molecules. Among various metal hydroxides, Ni $(OH)_2$ has been found to promote dissociation of water and hydrogen generation. A tremendous synergic effect exists when Ni $(OH)_2$ is combined with Pt. Capitalizing on this fact, H. Liu et al. prepared Pt-decorated Ni $(OH)_2/CeO_2$ as a hybrid electrocatalyst. The Pt NPs with an average size of 3.1 nm are homogeneously deposited on the Ni $(OH)_2/CeO_2$ (abbreviated as NC) nanosheets, which could increase the exposure area of active sites and improve the utilization of Pt. Additionally, the mosaic-structured NC nanosheets not only effectively catalyze the OER but also enhance the HER activity of Pt due to electronic modulation and promoted dissociation of water. The as-prepared PNC hybrid possessed an overpotential of 76 mV for HER and 186 mV for OER at 100 mA cm^{-2}. The PNC hybrid demanded a cell potential of 1.45 V to attain 10 mA cm^{-2} in 1 M KOH. The calculated turnover frequency (TOF) of the PNC hybrid was found to be 3.488 s^{-1}, remarkably performing better than Pt/C (0.455 s^{-1}) and Pt/G (0.254 s^{-1}). In addition, the PNC hybrid was found to perform well at high current density with fast formation and liberation of bubbles without any catalyst degradation, which seems suitable for industrial utilization. In an extended stability test, a constant potential of 2.06 V was maintained for 85 h with minor degradation at the current density of 1000 mA cm^{-2}. This higher performance was attributed to the large scattering of platinum NPs plus the electronic interaction between CeO_2, Ni $(OH)_2$, and Pt. In contrast, the stability enhancement was attributed to the strong deposit/graphite adhesion, hydrophilicity of the electrode, and aided release of gas bubbles [41]. Thus, alloying Pt with 3d transition metals serves as a prominent strategy for boosting the catalytic activity by enhancing the electronic and geometric structures of Pt. Furthermore, platinum electrocatalysts, including Pt–M alloys (M = transition metals, transitional metal chalcogenides/carbides/phosphides), have also been extensively investigated for efficient catalysts [42–45]. Therefore, Pt-based electrocatalysts are produced by lowering the amount of Pt while retaining electrochemical activity and stability. It is also known that nickel oxides or hydroxides catalyze the breakage of water molecules, producing H intermediates that adsorb on neighboring Pt to form H_2 [46–50]. As a result, Ni-based electrocatalysts serve as favorable electrocatalysts for OER and Pt for HER. Hence, it is advantageous to fabricate PtNi alloy nanoparticles as bifunctional catalysts for overall water splitting. Recently, X. Chen et al. electrodeposited a trace amount of Pt on $NiFeO_xH_y$ film with a copious amount of Ni^{3+} structure to improve the performance of water electrolysis. The Pt particles with a size of several nanometers are dispersed uniformly in $NiFeO_xH_y$ film. The short-brush $NiFeO_xH_y$ film undergoes easier surface transformation than nanosheets to form an active $NiFe(OOH)_x$ phase during OER activation. During OER activation, the $NiFeO_xH_y$ facilitates surface modification, forming $NiFe(OOH)_x$ phase, as it reached 10 mA cm^{-2} with an overpotential of 204 mV, performing better than typical $NiFeO_xH_y$ nanosheets. Furthermore, the Pt-modified materials possessed high Pt mass-specific activity and excellent HER catalytic activity with a cell potential of 1. 54 V, whereas commercial RuO_2 and Pt/C on NF required more than 1.65 V. For HER, the hybrid Pt/$NiFeO_xH_y$/NF catalyst resulted in an overpotential (η) of 48 mV, which remains lower than the $NiFeO_xH_y$/NF catalyst. Furthermore, a Tafel slope of 42 mV $decade^{-1}$ is observed for this catalyst. The low Tafel slope indicates that the Heyrovsky step, rather than the Volmer step, determines the electrocatalytic HER kinetics on hybrid Pt/$NiFeO_xH_y$/NF, demonstrating that the hybrid catalyst successfully stimulates water splitting in alkaline conditions. In the case of OER, this catalyst required an overpotential of 204 mV (@10 mA cm^{-2}), and their corresponding Tafel slopes were as small as 28 mV dec^{-1}, as shown in Fig. 2. Hence, this electrocatalyst performs better than the recently reported Ni-based compounds [46].

Similarly, through a simple and scalable corrosive-coordinate method, Chen et al. constructed a 2D-3D nanostructured hybrid with trace Pt (Pt-NiFe PBA) via a corrosion-coordination method. Herein, a 2D-3D nanostructure composed of metal hydroxides and Prussian blue analogous (PBA) was in situ decorated onto the NiFe foam (Pt-NiFe PBA) through a facile and scalable corrosive-coordinate approach. This specifically designed morphology favors the provision of abundant active sites, optimizes the reaction pathway, and accelerates mass transport during the electrocatalytic process. The as-synthesized catalyst required the overpotentials of 210 mV for OER and 29 mV for HER in an alkaline medium. Meanwhile, a favorable reaction kinetics was also evident with the Tafel slope, for HER value of 58.3 mV dec^{-1}, which was lesser in comparison to NiFe-LDH (148.9 $mVdec^{-1}$), NiFe PBA (124.3 $mVdec^{-1}$), and even Pt/C (67 $mVdec^{-1}$), and the corresponding OER value was 43.5 $mVdec^{-1}$. They suggested that the high performance may be attributed to a variety of factors, including coupling effects, specific nanostructure, binder-free feature, and hydrophilicity/hydrophobicity features, which resulted in favorable mass/charge transport, abundant exposed active sites, and improved reaction kinetics. Furthermore, to propel

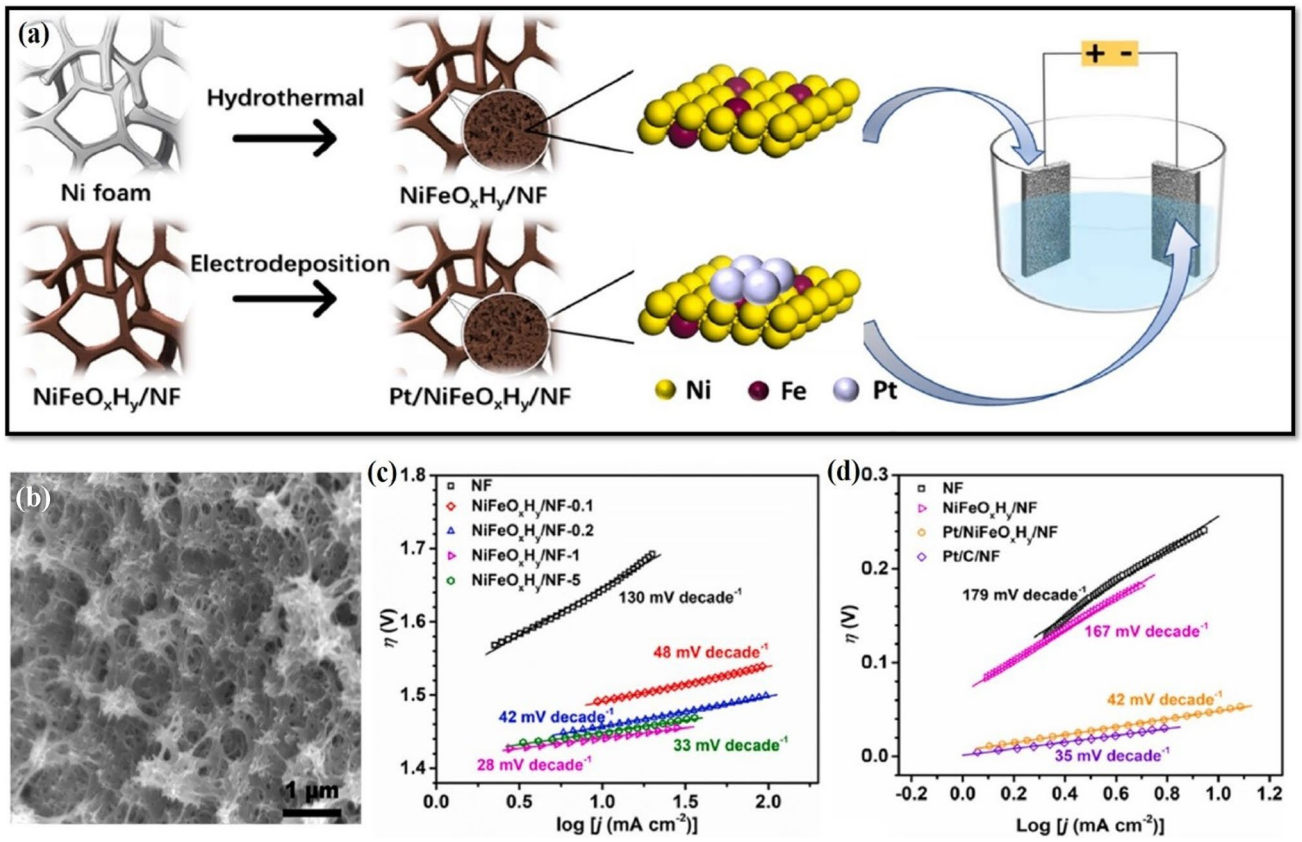

Fig. 2 **a** Schematic illustration of the synthesis process of the NiFeO$_x$H$_y$/NF and hybrid Pt/NiFeO$_x$H$_y$/NF electrodes, **b** SEM images of NiFeO$_x$H$_y$/NF-1 prepared on the Ni foam, **c** Tafel plots of the Ni foam and NiFeO$_x$H$_y$/NF samples, and **d** Tafel plots of Ni foam, NiFeO$_x$H$_y$/NF, Pt/NiFeO$_x$H$_y$/NF, and Pt/C/NF 49 reproduced with permission from ref. 50, copyright 2022, Applied Surface Science

forward from the traditional water splitting, they have set out a distinct experiment of approaching seawater electrolysis, which would be a suitable alternative. The electrocatalytic performance on 1 M KOH in seawater was excellent as it required the smallest overpotential of 21 mV to attain 10 mA cm^{-2} and 47 mV to 50 mA cm^{-2} [51]. Recently, layered double hydroxide has been focused as an electrocatalyst for water splitting. Several studies on catalytic water splitting with LDH-based materials as catalysts have been published, showing a fast growth trend [51–55]. This exposure to LDH was attributed to their abundance, lower price, and resource-richness compared to the activity and durability of traditional noble metals. Similarly, X. Zhang et al. anchored Pt clusters on NiMo hydroxide nanosheet via the chlorine etching method and found that this catalyst showed excessively high stability for 160 h. The SEM image indicated the formation of Pt clusters with an average size of 1.6 nm. These Pt clusters were found to be uniformly anchored on amorphous NiMo-OH/NF nanosheets. Regarding catalytic activity, the catalyst exhibited only a small overpotential of 34 mV (η_{10}) and 190 mV (η_{10}) for HER and OER, respectively. The high TOF number, mass activity, and ECSA proved their better HER performance. This excellent HER activity was caused by the collaborative electron transfer between platinum, nickel, and molybdenum. In terms of kinetics, the Tafel slope of Pt-NiMo-OH was 30.5 mV dec^{-1}, which was lesser than bare nickel foam (182.23 mVdec^{-1}) and Pt/C/NF (55.1 mVdec^{-1}). This better OER performance was attributed to the formation of high valence Mo and Ni, which was instrumental in the formation of OER active materials [56]. Y. Feng et al. also worked on platinum-nickel-based hydroxide. They synthesized vanadium-doped Pt clusters on NiFe-LDH (Pt-NiFeV) for overall water splitting. The continuous electrochemical CV cycling dissolutes Pt atoms from Pt net to get deposited onto the nucleation sites of the working electrode: defective NiFe-LDHs-Ar. Since the Fe and Ni atoms around the defect sites in NiFe-LDHs-Ar were active, the electrochemical cycling at negative potentials reduces the part of Ni and Fe ions. The Pt atoms diffuse from the counter electrode preferred to couple with the in situ reduced FeNi atoms to form PtFeNi alloys. Their research emphasized on the importance of doping vanadium in Pt clusters onto NiFe-LDH. The TEM analysis revealed that the self-reduced Pt nanoparticles on the NiFe-LDH nanosheets (Pt/NiFe) are

apparently larger than those in Pt/NiFeV, which indicates that V doping could prevent Pt overgrowth or agglomerate into large nanoparticles. This catalyst possessed a very high catalytic activity with an overpotential of 19 mV at 10 mA cm^{-2} and Tafel slope of 33 mV dec^{-1} for HER and 254 mV at 50 mA cm^{-2} and Tafel slope of 48 mV dec^{-1} for OER. This outstanding performance was also supported by DFT simulation, which showed that V doping modified the d-band center of Ni active sites, weakening the adsorption of *OH intermediates and facilitating the desorption of oxygen molecules at the anode. As a result of V doping, more electrons were transferred to neighboring Fe atoms, leading to an elevated reducing ability and optimized free energy of hydrogen adsorption and proton recombination kinetics at the cathode [57]. Combining an electrocatalyst with a support material results in significant advantages such as coalescence during electrochemical testing, which provides vital connections between nanoparticles and electrolytes, embeds the nanoparticles against detachment, and provides long-term stability against disintegration. Carbon nanofiber mats (CFMs) have recently gained much attention among the numerous carbon-based support materials because of their excellent mechanical stability, chemical resilience, and high electrical conductivity for charge transfer. D. Yin et al. proposed a Pt-WO_{3-x}@rGO hybrid composed of Pt, WO_x, and graphene. In this work, a new structure-defined cis-platin-modified Dawson-type POM complex of $K_6[P_2W_{17}O_{61}\{cis\text{-}Pt(NH_3)_2\}_2]\ 32H_2O$ ($P_2W_{17}Pt_2$) has been successfully fabricated by reaction of cis-platin and monolacunary Dawson-type POM. Then, through photochemical reduction, the in situ generated $P_2W_{17}Pt_2$@rGO hybrid can be achieved by anchoring POM on the reduced graphene (rGO) substrate. In the subsequent calcination process, the $P_2W_{17}Pt_2$@rGO hybrid forms a new ternary hybrid of Pt-WO_{3-x}@rGO, which exhibits excellent electrocatalytic water-splitting performance due to the combination of surface small Pt^0 nanoparticles on the WO_{3-x} substrate, which shows the better HER and OER activities. This catalyst demanded a cell potential of 1.55 V to attain 10 mA cm^{-2} in alkalinity. The spherical Pt^0 nanoparticles were widely dispersed on the WO_3 surface. The element analysis revealed a very low content of Pt, with a Pt ratio of 1.58%. However, this catalyst resulted in better performance for HER, with an overpotential of about 13 mV at 10 mA cm^{-2}, which was lower than 20% Pt/C catalysts (29 mV). Meanwhile, the prepared hybrid resulted in a trivial Tafel slope value (35 mV dec^{-1}) than the standard benchmark Pt/C (45 $mVdec^{-1}$). In the case of OER, the overpotential was 174 mV at 10 mA cm^{-2} in an alkaline medium. In addition, the low Tafel slope (48 $mVdec^{-1}$) confirmed the highest OER activity. In the alkaline condition, it exhibited a mass activity of 27 A mg^{-1} at an overpotential of 30 mV [58]. In addition, the performances of platinum-based electrocatalysts for water splitting are summarized in Table 1.

Table 1 Summary of platinum-based electrocatalysts for water splitting

Catalyst	Overpotential (mV)		Cell voltage (V)	Tafel slope ($mVdec^{-1}$)		Stability	Ref.
	HER	OER		HER	OER		
Pt–Cu@Cu_xO NWs/3DF	72	250	–	56	117	1000 cycles	[59]
Pt-decorated $Ni(OH)_2/CeO_2$	76	186	1.45	–	–	85 h	[41]
$NiFeO_xH_y$/NF-Pt	48	204	1.54	–	28	–	[46]
Pt/Ni_xFe LDHs	100	300	1.47	81.7	53.4	44 h	[60]
NiFe-LDH-Pt-ht	27	90	–	51	12	–	[61]
Pt-NiO/Gr-SUS	79	240	–	41	–	12 h	[62]
Pt-NiMo-OH/NF	34	190	1.47	–	–	160 h	[56]
Pt-NiFe PBA	29	210	1.46	–	43.5	12 h	[51]
Pt-NiFe-LDH/CC	28	228	1.57	–	69	40 h	[63]
Pt-Ni_3Se_2@NiOOH/NF	–	310	1.52	45	–	–	[64]
Ni–Fe–Pt nanocubes	463	333	–	81	65	1000 cycles	[65]
PtNiP MNs/C	54.4	320	1.590	39.3	49.8	2000 cycles	[66]
Ni–Mo@Pt-0.03	26	399	1.58	102.9	–	45 h	[67]
Pt_x@Ni_y-rGO	37	–	1.485	21.03	–	14 h	[68]
NF-Na-Fe-Pt	31	261	1.56	35.98	39.68	12 h	[69]
Pt/NiFeV	19	254	1.54	33	48	10 h	[57]
Pt QDs @Fe-MOF/NF	191	144	1.47	–	34	100 h	[70]
Co–Pt/C-10	50	320	–	152	75	10 h	[71]
PtNi/CNFs	34	151	–	31	159	10 h	[72]
Pt-WO_{3-x}@rGO	37	174	1.55	–	–	–	[58]

Palladium (Pd)-based materials

Palladium (Pd) nanocatalyst has recently been used as a replacement for platinum (Pt) nanocatalysts due to its increased electrocatalytic activity in alkaline conditions and availability. Palladium's electronic structure and catalytic activity can be manipulated by altering the local structure by alloying Pd with foreign metals or supporting Pd on metal oxides. Recently, S. Lu et al. identified a hitherto undiscovered two-dimensional palladium carbide using the structure swarm intelligence technique. The proposed monolayer, known as α-PdC, consisted of completely dispersed Pd atoms and a stiff carbon backbone with sufficient stability and strong electrical properties as suggested by theoretical calculation. As a result, it exhibited an excellent catalytic performance of about − 0.01 V (HER overpotential) and a low activation energy barrier (0.16 eV) [73]. In another study, Ipadeola et al. successfully anchored Pd nanocatalysts on chemically etched Ni metal-organic framework-derived carbon using microwave-assisted solvothermal synthesis. The resultant Pd/Ni/MOFDC reveals that the nanocatalysts' surfaces have flake-like morphology and exhibit better kinetics toward the HER and OER than the acid-treated nickel counterpart. This catalyst showed moderately improved kinetics and mass transport because of increased exchange current density ($j_{o,s}$ = 0.1079 mA cm^{-2}), lower activation energy (21 kJ mol^{-1}), and Tafel slope (b_c = 173.0 mV dec^{-1}) values. The high *j* values of the Pd/Ni/MOFDC toward alkaline HER may be traced to the strong synergy between Ni/$Ni(OH)_2$ interface and nanostructured Pd, as the Ni/$Ni(OH)_2$ can facilitate continuous H_2O cleavage with immediate desorption of Hads from the active sites of Pd, as well as prompt recombination of Hads making the Ni/$Ni(OH)_2$ interface beneficial for alkaline HER [74, 75]. H. Zhang et al. designed an N-doped PdCoNi composite (Pd-e-NiCo-PBA-C) via pyrolysis of a Prussian blue analogue. Furthermore, the composition was manipulated by an ion exchange technique, and its catalytic performance was explored. As a result, the morphology and structure of the Pd-e-NiCo-PBA-C change from a nanocube to a hollow nanocage and finally to tapered nanosheets. Impressively, encapsulation of $CoPd_2$ nanoparticles onto N-doped graphite carbon matrix successfully prevented the prevailing corrosion and resulted in the catalytic activity of more than 50 h of stability for total water disintegration, which was better than other twin-function electrocatalysts that have been recently reported. Meanwhile, when tested with LSV, it showed a minor shift after 5000 cycles, demonstrating excellent stability performance. The prepared electrocatalyst was tested in both alkaline and acidic conditions. As a result, the obtained electrode resulted in an overpotential of 47 mV at acidic conditions with a corresponding Tafel slope of 55 mV dec^{-1}. Furthermore, at the alkaline (pH = 14) condition, the overpotential of 147 mV and the corresponding Tafel slope of 67 mV dec^{-1} were achieved. For OER, this catalyst delivered the 10 mA cm^{-2} at overpotentials of 309 mV, which produced results comparable to those of commercial IrO_2 (343 mV) [76]. The electrochemical analysis revealed that the conductive graphite carbon matrix possessed various advantages such as electrolyte diffusion property, high specific surface area, and electronic configuration adjustment using nitrogen and nickel co-doping, accompanied by the distinctive dodecagon nanosheet morphology, which contributed to the exceptional HER performance. The significant OER activity, especially in acidic solutions, was attributed to the carbon conducting support with metallic composite, which provides a comparatively hydrophobic environment for electrocatalysts in acidic media. Karuppasamy et al. prepared defect-enriched palladium nanocrystals encapsulated on a half-hollow nanotube-structured N-MoO_2-Mo_2C (HHNT) heterointerface. The icosahedral Pd NCs finely encapsulated the N-MoO_2-Mo_2C surface with the average size of the icosahedral Pd NCs of approximately 48.5 nm.The obtained N-MoO_2-Mo_2C HHNT resulted in a significant boost in overall water solubilization activity. Furthermore, on assembly of the electrolyzer cell, this composite displayed a cell voltage of 1.56 V at a current density of 10 mA cm^{-2}. For HER, it demonstrated an overpotential of 65 mV at 10 mA cm^{-2}. The synergistic effect of Pd NCs and MoO_2-Mo_2C heterointerface was responsible for the remarkable electrocatalytic activity. Additionally, the Tafel slope was used to investigate the catalytic reaction kinetics and processes of HER electrocatalysts. On investigation, the Pd/N-MoO_2-Mo_2C resulted in a lower Tafel value of 46.1 mV dec^{-1} compared with Pt/C of 48.6 mV dec^{-1}. On the other hand, with the availability of active sites and unique structure, the Pd/N-MoO_2-Mo_2C electrocatalyst resulted in improved electrocatalytic performance with reduced activation energy. For OER, this as-prepared catalyst delivered a small overpotential (η) of 180 mV, and these results were considerably smaller than Pd icosahedral (η = 420 mV) and Pt/C (η = 440 mV). To further examine the interfacial reactions and kinetics of electrode, EIS was conducted, of which the lower R_{ct} value was responsible for the outstanding performances. The R_{ct} value of Pd/N-MoO_2-Mo_2C was 6.18 Ω, indicating more rapid electrode kinetics and increased catalytic activity. Here, the molar ratio of the produced O_2 and H_2 was determined quantitatively by gas chromatography and compared with the amount that had been theoretically calculated, where it was discovered to be 1.97:1 near to 100% Faradic efficiency [77]. W. Zhang et al. reported a method to hasten the hydrogen and oxygen evolution kinetics of NiFe-LDH by combining it with Pd-based material to form Pd/$NiFeO_x$ nanosheets. This catalyst was tested under various conditions and found that the catalyst showed excessively high stability for 50 h. In case 1 M KOH solution, the as-synthesized Pd/$NiFeO_x$ nanosheets exhibited

outstanding HER activity as it needed an overpotential of 76 mV and an overpotential of 180 mV in 0.5 M H_2SO_4 solution. Moreover, the catalyst attained a 10 mA cm^{-2} with overpotentials of 46 mV for HER and 169 mV for OER. Using 1 M phosphate-buffered saline (PBS) as an electrolyte, the catalyst exhibited a small overpotential of 75 mV (η_{10}) for HER and 310 mV (η_{10}) for OER. Because of the exceptional bifunctional activities of Pd/$NiFeO_x$ throughout a broad pH range, an electrolyzer was built using Pd/$NiFeO_x$ nanosheets as both anode and cathode to investigate the total water-splitting performance. The Pd/$NiFeO_x$||Pd/$NiFeO_x$ cell demanded a voltage of only 1.57 V to reach 20 mA cm^{-2} in 1 M KOH solution with nearly 100% faradic efficiency [78]. Furthermore, the HER and OER performance of palladium-based electrocatalysts for water splitting are given in Table 2.

Rhodium-based materials

Initially, Duan et al. reported a new rhodium phosphide (Rh_2P) nanocube with excellent HER and OER performance in an acidic solution [85]. Furthermore, Q. Qin et al. reported rhodium phosphide which exhibited excellent trifunctional activities for oxygen reduction, oxygen evolution, and hydrogen evolution reactions. Similarly, F. Yang et al. also found that the rhodium-based nanoparticles showed superior results in terms of HER. Likewise, Y. Zhao et al. prepared Rh nanosheets (Rh NSs) as bifunctional electrocatalysts for water electrolysis [86]. Thus, due to various advantages such as corrosion resistance, outstanding durability, anti-toxic nature, and strong electrochemical performance, metal rhodium (Rh) should be given special consideration as an electrocatalyst across various pH values. Recently, layered double hydroxide has received much attention as a catalytic material due to its good electrocatalytic stability. Among the hydroxides, nickel and iron hydroxides exhibit better catalytic activity for OER but poor HER. Therefore, H. Sun et al. prepared Rh-doped NiFe-LDH by the hydrothermal method, exhibiting nanosheet morphology. It demonstrates an overpotential of 24 mV and a Tafel slope of 27 mV dec^{-1} in an alkaline medium. The addition of Rh atoms to NiFe-LDH accelerates the dissolution of water molecules, improving HER performance. The improved kinetics were tested with EIS measurements. The low R_{ct} value demonstrated the involvement of a quick faradaic process and advantageous charge transfer kinetics. The intrinsic catalytic activity was examined with the help of electrochemical active surface areas. The ECSA of NiFeRh-LDH was normalized to be 1336.3 cm^{-2} (high), which could be due to the nanosheet nature of NiFeRh-LDH, as well as the vast number of oxygen vacancies, and availability of a large number of active sites. An overpotential of 204 mV was needed for oxygen evolution catalytic performance, which was much lower than NiFeVLDH, RuO_2, and IrO_2. The electrocatalytic performance of the as-prepared electrocatalyst is shown in Fig. 3. Furthermore, this catalyst was also excellent in urea electro-oxidation reaction (UOR), which was proved when the urine-mediated electrolysis cell required a potential of just 1.3 V for delivering a 10 mA cm^{-2} of current density. Additionally, the DFT calculation showed that the shift in the d-band center and the oxygen vacancies were responsible for the increased activity [39].

Cao et al. constructed a bifunctional catalyst for all pH values. Their strategy was to alloy noble metal with non-precious metal, reducing the high price and enhancing the electrochemical performance. Due to their higher electrocatalytic activity, they employed Cu-based 1D nanocrystals, especially nanotubes. In addition, the experiments and DFT calculations reveal that the formation mechanism of RhCu NTs is due to the etching of nanowires from both ends. The developed electrocatalyst resulted in various advantages such as increased interior and exterior active sites and preventing material aggregation. As a result, they

Table 2 Tabulation of HER and OER performance of palladium-based electrocatalysts

Catalyst	Overpotential (mV)		Cell voltage (V)	Tafel slope ($mVdec^{-1}$)		Stability	Ref.
	HER	OER		HER	OER		
PdP_2@CB	27.5	270	1.59	29.5	78.6	5000 cycles	[79]
Pd/MOFDC	35	–	–	–	–	–	[75]
Pd/$NiFeO_x$	180	76	1.57	78.03	59.18	50 h	[78]
Pd/N-MoO_2-Mo_2C	65	180	1.56	46.1	67.2	50 h	[77]
Pd-NP@MPC	95	–	1.65	62	–	50 h	[80]
Pd_3P/NPC	277	360	1.65	120	73	–	[81]
PdC monolayer (a-PdC)	10	360	–	–	–	–	[73]
RGO/MoS_2/Pd	86	245	–	35.9	42	–	[82]
Pd-e-NiCo-PBA-C	147	309	1.6	67	67	50 h	[76]
Pd-NiFe-LDH/NF	130	156	1.514	46	64	60 h	[83]
Palladium and cobalt based (PdCo)	78	310	–	42	73	71 h	[84]

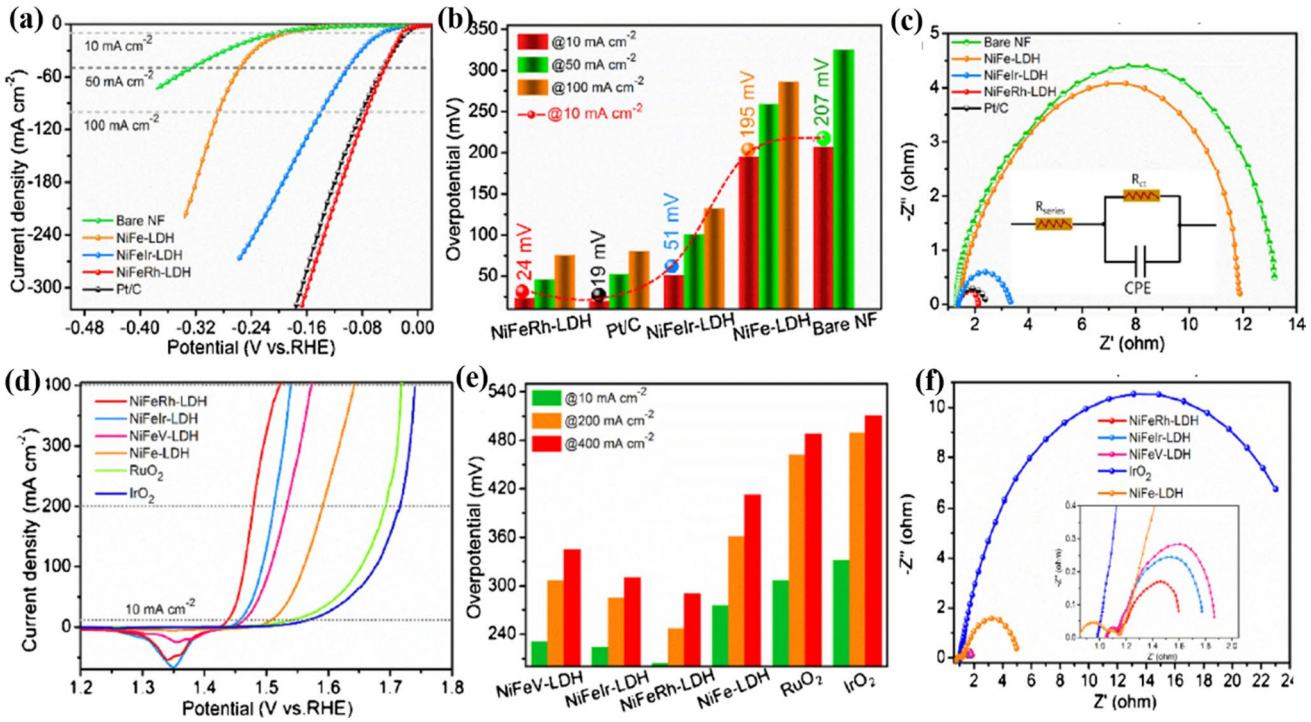

Fig. 3 Electrocatalytic HER properties. **a** Polarization curves of catalysts for HER (with iR compensation). **b** The derived overpotentials at 10, 50, and 100 mA cm^{-2} for the as-prepared catalysts. **c** Nyquist plots of the as-prepared catalysts. Electrocatalytic OER properties. **d** Polarization curves of catalysts for OER (with iR compensation). **e** The bar chart comparing overpotentials at 10, 200, and 400 mA cm^{-2}. **f** Nyquist plots of the catalysts86. reproduced with permission from ref. 86, copyright 2021, Applied Catalysis B: Environmental

synthesized defect-rich RhCu NTs via the wet chemical method. Specifically, the RhCu NT sample showed excellent HER activity with η_{10} of 8, 12, and 57 mV for 1 M KOH, 0.5 M H_2SO_4, and 0.1 M PBS conditions, respectively. As a result of the bigger exchange current density (j_0) and lower Tafel slope, RhCu NTs had higher activity and faster HER kinetics than Pt/C at all pH values. Furthermore, to investigate their extraordinary HER performance, DFT calculations were performed, which revealed that the HER amplification in an alkaline medium was due to the transition in electronic structure caused by higher Rh content [87]. Rare earth metal phosphides are commonly used in industry as catalysts for oxygen removal (HDO), nitrogen removal (HDN), sulfur removal (HDS), and other processes. This has prompted researchers to look into their usage in electrocatalysis. Among them, rhodium phosphide exhibits different crystalline phases and therefore shows an impressive electrocatalytic performance. X. Wu et al. in their experiment synthesized rhodium phosphide nanoparticles implanted in a nitrogen/phosphorus-doped carbon matrix with a very low Rh loading of 39.2 μg cm^{-2}. The resultant bifunctional electrocatalyst (Rh_2P-N/P-CC) outperformed well against Pt/C. In terms of stability for HER, after a time of 40 h only, a mere surge of 13 mV was observed at 100 mA cm^{-2}. This catalyst displayed significantly enhanced HER activity with an overpotential of 5 mV at 20 mA cm^{-2}. The Rh_2P-N/P-CC had a Tafel slope of 47 mV dec^{-1}, similar to Pt/C (49 mV dec^{-1}), showing a kinetically accelerated HER process. Similarly, the required overpotentials for OER was 274 mV to achieve a current density of 20 mA cm^{-2}. The sensible integration of its unique structural and compositional characteristics resulted in its exceptional electrocatalytic performance. Thus, Rh2P nanoparticles proved to be efficient electrocatalysts with minimal loading of Rh, with their uniform distribution and partial attachment of the doped atoms significantly improving stability at high current density electrolysis [88]. Due to their huge specific surface area, rich coordinated atom content, and high density of edges and flaws, two-dimensional is the most alluring electrocatalyst for accelerating water electrolysis. The intrinsic properties of graphene-based materials, such as graphene as an electroactive component, reduced graphene, graphene quantum dots, doped graphene, and functionalized graphene supports, have attracted a lot of interest in the catalysis field, and have shown particular promise in water electrolytic application. Narwade et al. developed a hybrid electrocatalyst of rhodium nanoparticles decorated onto graphene oxide with elevated exposure to active Rh nanosphere (NS) sites. For HER, the faster kinetics can be proved by the smallest Tafel slope of 10 mV dec^{-1}, Rh−GO catalyst showed majestic HER

activity, as it possessed a minute overpotential of 2 mV at 10 mA cm^{-2}. To further probe the activity of this, catalyst electrochemical impedance spectroscopy (EIS) was used. The R_{ct} values of 6.6 Ω indicated the substantial enhancement in electron transport during HERs in acidic media. In OER studies, the catalyst reached 10 mA cm^{-2} at an overpotential of 0.23 V and provided a Tafel slope of 27 mV dec^{-1}. These outcomes supported hydroxyl regeneration poisoned by Rh, resulting in excellent performance and reduced hydrogen production cost via electrolysis. This outstanding performance was attributed to the decoration of Rh NSs onto GO, which increased viability toward interfacial electron transfer [89]. In addition, the HER and OER performances of rhodium-based electrocatalysts are summarized in Table 3.

Iridium-based materials

Combining Ir with non-noble metals is not only an effective way to reduce Ir consumption, but it also has the potential to change the electronic structure and adsorption energy, resulting in increased intrinsic activity for water splitting. R. Fan et al. doped Ir with NiCo-layered double hydroxide via the solvothermal method. The FESEM image of the Ir-NiCo LDH exhibits homogeneously distributed bright dots (~ 0.2 nm), confirming the presence of single Ir atoms dispersed in the NiCo LDH nanosheets. This as-synthesized Ir-NiCo LDH on NF demonstrated an exceptional long-term stability of over 200 h, which makes it the best among Pt/C||Ir/C couple and other recently reported bifunctional catalysts. This can be ascribed to the following two factors: (1) Ir-NiCo LDH's lattice, Ir atom existed as independently scattered single atoms. Single-atomic Ir in Ir-NiCo LDH was remarkably stable due to the strong electrical connection between the iridium atom and the NiCo LDH, which played a vital role in increasing catalyst stability under working conditions. (2) Significant crystal defects like OVs were found due to spontaneous galvanic displacement between NiCo LDH and Ir precursor. The as-prepared catalyst displayed an exceptional catalytic activity for its application. To achieve 10 mA cm^{-2}, overpotentials of 21 mV (for HER) and 192 mV (for OER) were required. Moreover, their resultant Tafel slopes were only 35 mV dec^{-1} and 41.2 mV dec^{-1}. The Ir-doped NiCo LDH electrocatalyst achieved an extraordinary performance with a modest cell voltage of 1.45 V in an alkaline medium due to synergistic effects in the HER and OER process, along with the ECSA and enhanced electrical conductivity. Additionally, EIS studies were employed to understand better the kinetics related to catalytic activity. With the help of the Nyquist plot, it was found that the Ir-NiCo LDH exhibited only minor charge transfer resistance R_{ct} of 0.65 Ω. Thus, the complete water-splitting efficiency of the Ir-NiCo LDH coupling was assessed. Furthermore, in the case of the water electrolysis carried out for 90 min, the Faradaic efficiency was approximately 100% [96]. To improve the catalytic performance, interface control has recently received much attention. The creation of defect active sites results in improved electrocatalytic activity, which might be greatly enhanced by homointerface. Homointerfaces are believed to cause defects due to lattice distortion, which is critical for enhancing electrocatalytic activity. Investigating this distinctive morphology of Ir-based materials is crucial for enhancing electrocatalytic water-splitting performance. Gao et al. developed homointerface $IrCo_x$ nanorings (NRs) with bracelet-like architecture using a simple, controlled, surfactant-free method. The nanoring-structured $IrCo_x$ was synthesized by combining reduction and an etching process. With the help of EDX, it was confirmed that the bracelet-like $IrCo_x$ morphology was formed with ample homostructure interfaces. The LSV shows that, when compared to the C-$IrCo_{0.14}$, the $IrCo_{0.14}$ nanowire had an enhanced HER performance, with an overpotential of 16 mV and a corresponding Tafel slope of 28.8 mV dec^{-1}, showing improvement in HER activity and reaction kinetics. Likewise, for OER, the anodic reaction reached an overpotential of 278 mV at 10

Table 3 Summary of HER and OER performance of rhodium-based electrocatalysts

Catalyst	Overpotential (mV)		Cell voltage (V)	Tafel slope ($mVdec^{-1}$)		Stability	Ref.
	HER	OER		HER	OER		
Rh_1Sn_2/SWNT	46	312	1.56	81.11	71.69	5000 cycles	[90]
Rh NSs on graphene oxide	2	0.23	–	10	27	–	[89]
RhCu NTs	8	315	–	40	86	12 h	[87]
Rh_6Cu_1 NCs	17	300	1.55	29	70	10,000 cycles	[91]
Rh/NiFeRh-LDH	58	–	1.46	81.3	40	–	[92]
NiFeRh-LDH	24	290	1.455	27	29	80 h	[39]
Rh-doped CoFe-ZLDH	28	245	1.46	42.8	–	–	[93]
Echinops-like Rh PNNSs	–	79.5	1.61	55.1	–	–	[94]
Rh_2P-N/P-CC	5	274	1.7	47	61	40 h	[88]
Fe, Rh-Ni_2P/NF	73	226	1.62	–	52.7	–	[95]

mA cm^{-2} [97]. In addition, Fig. 4 indicates the (a) schematic of the solar water-splitting system in 0.1 M $HClO_4$ and (b) photos of an electrolyzer device powered by a Si cell in 0.1 M $HClO_4$.

Similarly, J. Chen et al. synthesized an iridium-iron alloy with a volcano-like morphology, providing a high specific surface area and abundant active sites to enhance catalytic activity. This distinctive volcano-like morphology FeIr alloy was grown hydrothermally with 0.546 wt% Ir loading. This material presented exceptional catalytic activity and stability for HER, OER, and overall water splitting. The bifunctional electrocatalyst possessed an overpotential of only 220.0 and 25.6 mV for OER and HER, respectively. Even at an elevated current density of 1000 mA cm^{-2}, the overpotentials are only 327.0 mV (HER) and 410.0 mV (OER) with exceptional stability and negligible declines after being maintained for 124 h. As soon as the HER long-term stability test was complete, the SEM pictures and HRXPS spectra were analyzed. Its outstanding stability is evidenced by the fact that the structural and elemental states were maintained. Thus, water splitting required 1.51 and 1.75 V to arrive at 10 and 500 mA cm^{-2}. Furthermore, it was operated at 500 mA cm^{-2} for 100 h in 30 wt% KOH solution at 60 °C, which seems useful for widespread applications. Thus, the excellent performance was predominantly due to (i) Fe and Ir alloying that improved the inherent catalytic activity, (ii) a distinctive volcano-like structure that provided adequate active sites, and (iii) a self-supporting structure that maintained superior stability [98]. The synthesis process of the as-prepared FeIr alloy is shown in Fig. 5.

Recently, multi-metal oxides formed by the combination of iridium and metal serve as a promising strategy to address insufficient activity and stability of Ir as an electrocatalyst [99–101]. Many Ir-based 3D perovskites ($AIrO_3$), where A represents an alkaline-earth/alkaline/ metal ion, have been investigated recently. L. Zhang et al. constructed strontium

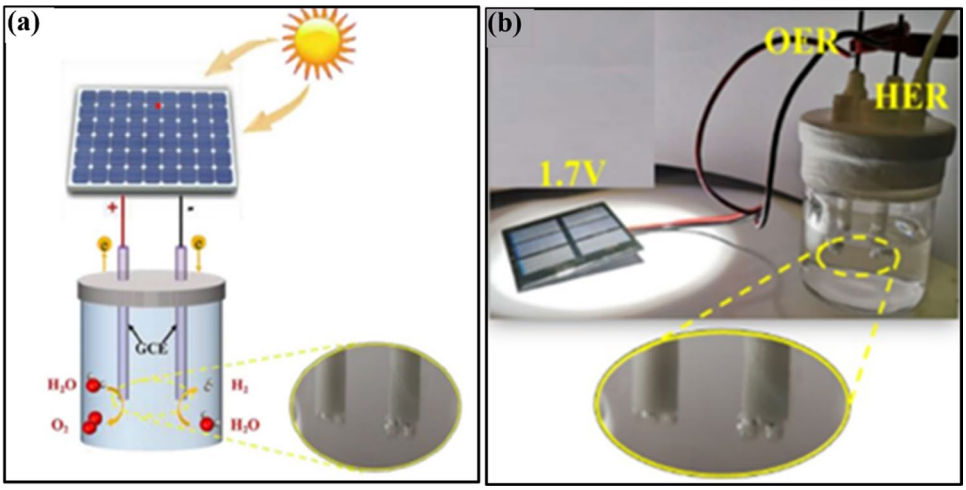

Fig. 4 **a** Schematic of solar water-splitting system in 0.1 M $HClO_4$. **b** Photos of full water-splitting device powered by a commercial Si cell in 0.1 M $HClO_4$ [97], reproduced with permission from ref. 97, copyright 2020, Electrochimica Acta

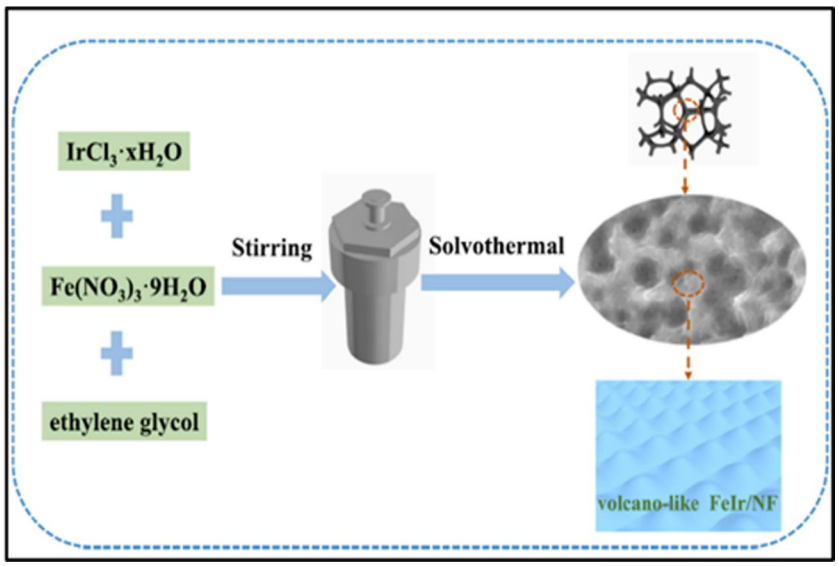

Fig. 5 Schematic representation of synthesis illustration of volcano-like FeIr/NF [98] reproduced with permission from ref 98, copyright 2021, Chemical Engineering Journal

iridate perovskites, SrIrO (laminar Sr_2IrO_4 modified with 6H phase $SrIrO_3$) [34]. The in-plane corner-shared IrO_6 octahedral framework's structural stability after cation leaching was improved, improving its stability during catalysis, as shown in Fig. 6. This is because of the layered nature of the material, which makes it easier for the cations (interlaminar) to be extracted without changing that structure's fundamental makeup. The deformed monoclinic hexagonal structure of the 3D 6H $SrIrO_3$ has been theoretically and experimentally shown to be more active for the OER.

Taking advantage of the benefits, the as-prepared SrIrO catalyst exhibited exceptional catalytic activity, with an overpotential of 18.2 mV at 500 mA cm^{-2}. A layer of IrO_x with IrO_6 octahedral structure domains was generated on the surface during the testing. As a result, it is inferred that SrIrO's extraordinary HER activity was predominantly due to the as-fabricated IrO6 octahedra-dominated IrO_x layer after Sr leaching. As a result, higher HER activity during continuous HER tests was due to metallic Ir's occurrence on the catalyst surface. As a result, SrIrO-1100 resulted in a better Tafel slope value of about 30.6 mV dec^{-1}, which was near to the benchmark Pt/C (27.5 mV dec^{-1}), showing that it had quick response kinetics that proceeds via the Volmer-Tafel reaction mechanism. In a full cell analysis for total water splitting, SrIrO endowed a small cell potential of 1.50 V at 10 mA cm^{-2}, significantly superior to most electrocatalysts in an acidic environment [102, 103]. Recent studies have shown that combining iridium with 3d transition metals can manipulate the electronic structure of Ir by improving the intrinsic activity and reducing the usage of Ir. Meanwhile, doping a heteroatom within carbon materials plays a significant role in stability by modifying electronic structures and interacting metal with support. As a result of this foresight, Z. Zhang et al. achieved a record-low overpotential of 4.7 mV@10 mA cm^{-2} with Ir/Fe@NCNT (Ir content = 4 wt%) composite for cathodic reaction. The catalyst was synthesized by pyrolyzing ferric chloride, melamine, and iridium trichloride to obtain Ir(20)/Fe@NCNT-900. High standards were maintained well in terms of the kinetic behavior of the as-prepared catalyst. A conclusion was reached that both Ir(20)/Fe@NCNT-900 and Pt/C have approximately closer Tafel values. Another cardinal parameter for evaluating kinetics was the R_{ct} value. The R_{ct} value of 0.93 Ω was obtained from the Nyquist plot, indicating its rapid charge transfer during the HER. Meanwhile, the turnover frequency (TOF) was estimated to be 6.65 s^{-1}, superior

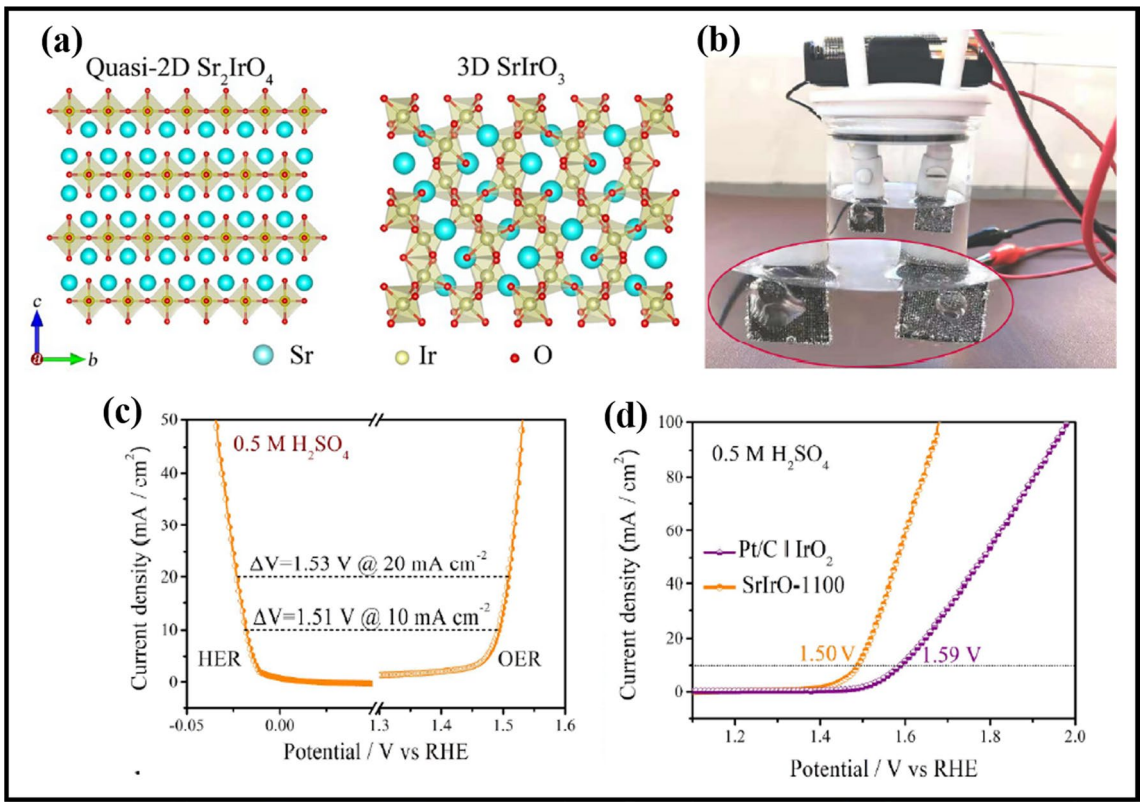

Fig. 6 **a** Crystal structures of quasi-2D Sr_2IrO_4 and 3D $SrIrO_3$. **b** SrIrO-1100-based two-electrode electrolyzer driven by a battery of 1.5 V. **c** LSV curves for OER and HER in 0.5 M H_2SO_4. **d** The overall water-splitting LSV curves for SrIrO-1100 and commercial IrO2‖Pt/C in 0.5 M H_2SO_4 [34] reproduced with permission from ref 102 copyright 2021, Chemical Engineering Journal

to the reported Ir-based catalysts. This indicates that Ir(20)/Fe@NCNT-900 has a high intrinsic activity for OER. As a result, this outstanding performance was aroused from the synergistic effect of NCNT, Fe, and Ir species. Thus, the NCNTs serve as conductive support and armor, shielding the metals from direct contact with the electrolyte. In the case of Fe, the Ir–Fe interaction helped optimize the iridium's electronic structure, making OER and HER thermodynamically easier. The Ir–Fe interaction and the wrapping of NCNT limited the aggregation and dissolution of atomically distributed Ir. Thus, the two forms (atomically distributed Ir in the Fe nanoparticle lattice and Ir nanoclusters on NCNT) generated enhanced active sites for HER and OER, including the Ir^0 and Ir^4 species. Furthermore, the HER and OER performances of iridium-based electrocatalysts are summarized in Table 4.

Ruthenium-based materials

Reier et al. studied the activity and stability of the oxides of Ru, Ir, and Pt nanoparticles along with their bulk counterpart. The electrocatalyst activity of these nanoparticles decreased in the order of oxidized Ru > oxidized Ir > oxidized Pt. The Pt nanoparticles experienced extra deactivation compared to the bulk catalyst, making them an inferior candidate [122]. Ruthenium (Ru) plays a significant role in electrocatalysis because of its lower cost and similar HER activity of Pt. Cen et al. synthesized a Ru-doped NiCoP nanowire catalyst for high-performance overall water splitting. The unique 3D interconnected nanowires ensure the uniform distribution of Ru coupled with NiCoP and endow the Ru-NiCoP/NF with the large ECSA, fast electron transport, and favorable reaction kinetic attributes. In addition to high intrinsic activity and a large number of accessible active sites, the Ru-NiCoP/NF catalyst also has improved electron transfer and expedited reaction kinetics in catalytic processes. As a result of this, the electrocatalyst provided better catalytic activity as it needed only 32.3 mV at 10 mA cm^{-2} and 233.8 mV at 50 mA cm^{-2} for HER and OER, respectively, with higher activity than the earlier reported electrocatalysts. The corresponding Tafel slope was analyzed to provide insight into the HER kinetics. This catalyst has a very low Tafel slope compared to other control samples, such as bare Ni foam. Furthermore, the enhanced HER activity was reassured by the higher value of C_{dl} obtained from ECSA, which was due to higher exposed active sites. In an

Table 4 Tabulation of HER and OER performance of iridium-based electrocatalysts

Catalyst	Overpotential (mV)		Cell voltage (V)	Tafel slope ($mVdec^{-1}$)		Stability	Ref.
	HER	OER		HER	OER		
IrW nanobranches	16	271	1.58	31.4	66.3	16 h	[104]
IreCo electrocatalysts	108	–	–	36	–	10 h	[105]
Ir/GF	7	290	–	30	46	2000 cycles	[106]
Ir-NS	133	254	1.51	72.5	–	1000 cycles	[107]
SA-Ir@GS	–	–	1.65	88.4	–	5 h	[108]
Ir-NR/C	–	290	–	20.3	72.4	–	[109]
$IrCo_{0.14}$ NRs	16	278	1.53	28.8	41.7	14 h	[97]
Si–Ir	114	343	–	36.5	–	–	[110]
Volcano-like FeIr/NF	25.6	220.0	1.51	50.46	64.78	124 h	[98]
Au@$AuIr_2$	29	–	1.55	15.6	–	40 h	[111]
Ir_xCo_{1-x} alloy nanotubes	6	246	–	25.1	–	2.7 h	[112]
AuIr@CNT	27.3	257	1.51	30.2	77.6	50 h	[113]
SrIrO	18.2	245	1.50	30.6	47.4	40 h	[34]
Ir-$Co_xNi_{1-x}O$/NF	53	260	1.55	70	48		[114]
$Ir_xMn_{(1-x)}O_y$ & L_{12}-$IrMn_3$ hybrid	36	–	–	31.6	–	–	[115]
($Ni_{0.93}$ $Ir_{0.07}$ /rGO)	32.5	271.8	1.52	137.1	55.9	24 h	[38]
Ir(20)/Fe@NCNT-900	4.7	300	1.52	31.9	64.5	4 h	[116]
NiIr@N-C/NF	32	329	1.50	107.5	82.2	10 h	[33]
Ir@N-G-750	19	303	1.6	26	50	–	[117]
Ir@N-G-600	92.5	327	–	41	74	28 h	[118]
Ir/N-rGO	76	260	1.74	45.8	60.4	25 h	[119]
Ir-SA@Fe@NCNT	26	250	1.51	31.8	64.8	12 h	[120]
Ir/WO_x/rGO	53	265	1.53	43	62	–	[121]
Ir-doped NiCo LDH	21	192	1.45	33.2	41.2	200 h	[96]

aqueous electrolyte, the OER produces a current density of 50 mA cm^{-2}; a small overpotential of 233.8 mV was required. According to the EIS Nyquist plots, the R_{ct} value of this catalyst was less, which implied that it could transfer charge more rapidly for OER. A full cell evaluation was carried out as part of the three-electrode studies. Furthermore, the electrolyzer cell was tested for 140 h at a current density of 100 mA cm^{-2}, demonstrating that the prepared catalyst possessed exceptional long-term stability for water-splitting applications. Moreover, the Faraday efficiency was investigated by comparing the theoretical and actual gas volumes at a constant current density of 25 mA cm^{-2}. For H_2 and O_2 evolution, the Ru-NiCoP/NF catalyst has nearly 100% [123]. Likewise, doping noble metal with transition metal dichalcogenides is the best technique. Layered 2H-molybdenum sulfide (MoS_2) has attracted attention due to its unique structural and electronic properties. Additionally, 1T-MoS_2 has an edge-rich structure, which produces a high ratio of exposed surface atoms and an ultrahigh specific surface area, which increases the HER catalytic activity. This is reflected in a recent pioneering study by Maiti et al., where they fabricated a Ru-doped CuO/MoS_2 (MSCR) hybrid. The electrochemical measurement revealed a distinct activity in the case of cathodic investigation with an overpotential of 198 mV. Furthermore, the as-prepared catalyst exhibited a Tafel slope of 113 mV dec^{-1}. In the case of anodic examination, the MSCR hybrid catalyst exhibited a superior overpotential (201 mV at 10 mA cm^{-2}) and Tafel slope (229 mV dec^{-1}). Additionally, an increase in the active sites of hybrid was due to the combination of copper oxide and ruthenium which helped in improving MSCR hybrid catalytic activity. Furthermore, with the help of cyclic voltammetry (CV) and electrochemical active surface area (ECSA), the various performance indexes such as C_{dl} and R_f were found. From this, they conclude that the astonishingly high double-layer capacitance, large electrochemical active surface area, and significant roughness factor of the MSCR hybrid in the alkaline medium could be attributable to its robust OER performance [124]. Precious metal aerogels have recently gained much attention due to their higher electrical conductivity, porous nature, and several hundred active sites for electrochemical applications. Taking advantage of this fact, S. Yan et al. demonstrated the development of a three-dimensional ruthenium (Ru) aerogel with a unique porous structure in alkaline and acidic conditions, resulting in better electrocatalytic water-splitting performance compared to Pt/C. As a result, ruthenium aerogel delivered the overpotential of 36 mV, which was better than Ru, Ru-60, and 20% Pt/C catalyst. In addition, in an alkaline environment, the HER behavior followed the Volmer-Tafel mechanism. As a result, the thermodynamic energy barrier to the HER lowers, leading to increased catalytic activity. Moreover, the Ru-30 required a cell potential of 1.48 V to achieve 10 mA cm^{-2} and stay stable [125]. Meanwhile, B. Yang et al. reported RuCoP nanoparticles in nitrogen-doped carbon, which presents rhombus faces and straight edges and is labeled as RuCoP@CN. This catalyst was engineered by in situ carbonization with the template ZIF-67. Transmission electron microscopy was utilized to comprehend the influence of structure on catalytic performance; Ru atom addition caused an increase in the number of lattice fringes of RuCoP. Thus, RuCoP@CN electrocatalyst affords an overpotential of 24 mV. Furthermore, to investigate the intrinsic catalytic activity, ECSA was employed. The C_{dl} value of RuCoP@CN was found to be 133 mF cm^{-2}. Furthermore, the exchange current density (j_0) was calculated by an extrapolation method from the Tafel slope. Overwhelmingly, RuCoP@CN exhibited more activities than the others, benefiting from the existence of P and Ru atoms. Furthermore, the RuCoP@CN could retain 100 h of stability during the overall water done by chronopotentiometry. According to DFT simulations, Ru and P doping could optimize the free energy and promote electron enrichment for HER and OER [126]. Cen et al. synthesized a hybrid electrocatalyst comprising Ru-MoO_{3-x} NF. Additionally, comparative studies were conducted to demonstrate that urea is crucial for the creation of unique structures, morphologies, and metal reduction. As a result, the as-prepared hybrid resulted in the overpotential of 12 mV at 10 mA cm^{-2}, 49 mV at 100 mA cm^{-2}, and high endurance of at least 17 h in alkaline conditions. In addition, the MoO_{3-x} with oxygen deficiency provided larger active sites and improved intrinsic activity, facilitated electron transport, and successfully prevented the loss of Ru species during the catalytic process. Therefore, the as-prepared electrode exhibited better HER performance. Furthermore, on assembly of electrolyzer cells using Ru-MoO_{3-x} NF and Fe_3O_4-NiFe-LDH NF, the cell voltage of 1.46 V was acquired and demonstrated high stability without obvious activity loss after continuous operation of 180 h [127]. Pei et al. synthesized Ru loaded on nickel foam (Ru/NF) by substitution reaction, which exhibited an outstanding bifunctional catalytic performance with reasonable overpotential and better reaction kinetics, superior to commercial Pt/C. This catalyst labeled Ru/NF was prepared by wet chemistry strategy with only 0.3 wt% of Ru loading, endowed with an HER overpotential of 10 mV and Tafel slope of 34 mV dec^{-1}. Due to their better catalytic activity, the complete water-splitting system was tested directly with Ru/NF-2 as the anode and cathode. It offered an applied cell voltage of 1.56 V to accomplish 10 mA cm^{-2} without visibly declining performance. The superior performance can be accredited to the addition of Ru, which causes the d-band of Ru/NF to move to the Fermi level, modulating the surface adsorption properties of the reaction intermediate (H*). Likewise, adding Ru increased the adsorption of H_2O onto the Ru/NF surface, resulting in a quick Volmer step. These findings show that the Ru/NF has incredible

potential for HER. In the case of OER, the formation of O–O bonds are favored by electron transport between Ru and Ni substrates. Adding NiO_x or other oxides to the catalyst's surface boosted its OER performance, which proved an effective method. Furthermore, Ni^{2+} on the surface of Ru/NF increased the water splitting, while Ni^{3+} on the surface stimulated the production of oxides and hydroxides (NiOOH), providing more OER active sites [128]. J. Zhang et al. produced an extraordinary result of an ultralow overpotential of 2.04 mV at 10 mA cm^{-2} for hydrogen evolution reaction in alkaline media. They constructed RuCoFe nanosheet (RuCoFe NS) via a rapid heating strategy. The electrochemical testing showed that RuCoFe NSs required only 180 mV of overpotential to reach 10 mA cm^{-2}. This impressive performance was again proved when the Tafel slope value (69.18 mV dec^{-1}) was revealed. Stability is another important attribute to consider when evaluating the performance of OER electrocatalysts. Even more unexpectedly, RuCoFe NS OER activity has not changed after 5000 cycles. As mentioned earlier, they achieved 2.04 mV@10 mA cm^{-2} in terms of the cathodic process of water splitting. Furthermore, it also exhibited outstanding kinetics and durability as it possessed a Tafel slope of 33.07 mV dec^{-1} and sustained 5000 cycles of ADT test using cyclic voltammetry and the typical chronoamperometry. The two-electrode device has good catalytic performance as it reached a current density of 10 mA cm^{-2} with just 1.56 V [129]. Furthermore, the HER and OER performances of ruthenium-based electrocatalysts are summarized in Table 5.

Inter-noble materials

It is well known that RuO_2 and IrO_2 are promising catalysts for acidic OER. However, RuO_2 has the disadvantage of having low stability in acidic conditions at high potential. To improve the stability of acidic OER, Shan et al. reported that strained Ru core and IrO_x shell heterostructures with significant charge redistribution can act as stable catalysts for acidic OER [149]. To further investigate the stability issue, J. Wang et al. reported the single-site Pt-doped RuO_2 hollow nanospheres (SS Pt-RuO2 HNSs) with interstitial C, which serves as highly active and stable electrocatalysts

Table 5 Summary of HER and OER performance of ruthenium-based electrocatalysts

Catalyst	Overpotential (mV)		Cell voltage (V)	Tafel slope (mVdec^{-1})		Stability	Ref.
	HER	OER		HER	OER		
Ru-MoO_{3-x} NF	12	216	1.46	32.9	42.42	180 h	[127]
Ru/Cu-doped RuO_2 complex	142	–	1.47	56	–	40 000 s	[130]
Ru-CoO_x/NF	252	370	–	28	134	100 h	[131]
Ru-CoO_x/NC	73	210	–	61.18	11	100 h	[132]
Ru aerogel	24	372	1.467	14	42	5000 cycles	[125]
RuO_2/NiO	22	250	–	31.7	50.5	24 h	[133]
RuO_2/Co_3O_4−RuCo@NC	141	247	1.66	63	89	–	[134]
RuCu NSs/C	20	234	–	–	–	45 h	[135]
Amorphous RuCoFe nanosheets	2.04	180	1.56	33.07	–	5000 cycles	[129]
$RuNi_1Co_1$@CMT	78	299	1.58	77	83	30 h	[136]
Ru-NiCoP/NF	32.3	233.8	1.50	60.9	52.66	140 h	[123]
MIL-53(Ru-NiFe)@NF	62	210	1.6	–	42	18 h	[137]
Ru-doping of $NiCo_2O_4$ spinel (NCO)	109	–	–	22	–	100 h	[138]
La-doped RuO_2	71	208	1.53	49.3	57.4	28 h	[139]
Ru-doped NiO/Co_3O_4	138	269	–	58	59	>40 h	[140]
Ru-CoV-LDH@NF	32	230	1.50	36.4	81.2	48 h	[141]
Ru–Fe_3O_4@FeNi–LDH/IF	104	189	1.52	86.5	34.3	36 h	[142]
Ru/Ni_3N-Ni	53	200	1.49	–	56.4	20 h	[143]
Ru shell and a Ru-Ni alloy core	39	252	–	53.9	–	12,000 cycles	[144]
Ru/Ni	10	–	1.56	34	–	20 h	[128]
Ru@Ni-B	14	–	1.42	111.8	180	–	[145]
Ru-RuO_2-NC	112	176	1.55	–	61	80 h	[146]
Ru@Ni-B	14	180	1.42	111.8	82.0	72 h	[145]
Ru_2Ni_2 SNs/C	40	23	1.45	23	–	40 h	[147]
RuCoP@CN	24	362	1.60	98	107	100 h	[126]
RuO_2/F-graphene	49	239	1.56	52	31	90,000 s	[148]

for overall water splitting. They have addressed the durability issue, where this as-prepared catalyst exhibited better stability for more than 100 h at 100 mA cm^{-2}. Additionally, the catalytic efficacy of this catalyst during OER was outstanding, showing minor overpotentials of 228 mV to achieve 10 mA cm^{-2} and 282 mV for reaching 100 mA cm^{-2}. Concerning HER performance, at current densities of 10, 50, and 100 mA cm^{-2}, the overpotentials were 26, 47, and 67 mV, which matches the Pt/C catalyst. The experiments show that interstitial C can lengthen the M–O bonds (where M = Ru and Pt) and the added single-site Pt has a considerable impact on the electrical interaction of RuO_2. According to theoretical calculations, the strong synergy promotes OER performance by lowering energy hurdles and increasing the dissociation energy of *O species [150]. Core/shell morphology has recently been widely investigated in many energy storage applications. Electrocatalytic studies were conducted on these structures, and the nature of the two underlying mechanisms such as ligand effect and strain effect was not elucidated clearly in prior research. Therefore, M. Li et al. prepared precise PdCu/Ir nanocrystals with core/shell morphology. This study specifically tuned heteroepitaxial coating and monolayer (ML) Ir shells onto the PdCu nanocrystals to get the exclusive strained PdCu/Ir core/shell nanocrystals. In addition, it exhibited an OER overpotential of 283 mV corresponding to 10 mA cm^{-2} and high mass activity of 1.83 in acidic media, significantly superior to their non-strained alloy counterparts. DFT calculations further supported the predominance of compressive strain in improving activity by showing how it affects the adsorption strength toward oxygenated intermediates. The result was a very effective and stable electrocatalytic water-splitting electrolyzer with a cell voltage of 1.583 Vat 10 mA cm^{-2} for HER and a 20 mV toward HER overpotential reported by the strained PdCu/Ir core/shell nanocrystals [150]. High entropy alloys (HEAs) have gained attention as they can perform unique water-splitting catalytic processes. Even though there are several synthesis methods, the HEA nanoparticle produced has a common issue of uneven composition. As a result, Y. Lu et al. proposed an easy and quick approach to synthesize FeCoNiCuPtIr HEA nanocatalysts via pulsed laser irradiation, as depicted in Fig. 7. Pulsed radiation, on the other hand, prevented the Ostwald ripening phenomena by effectively controlling the size of HEA nanoparticles and accelerating reactions with its intrinsic hollow active sites (i.e., OER and HER), which showed an overpotential of 255 mV and a modest Tafel slope (61.7 mV dec^{-1}) in alkaline conditions for OER and an exceptionally small overpotential 21 mV and a small Tafel slope (54.5 mV dec^{-1}) for HER. Meanwhile, DFT studies revealed that adding Ir atoms reduces the coupling strength of adsorbate and alloy surface by donating valence electrons to surrounding hollow sites [150]. The most effective catalysts in PEM water electrolyzers are Ir- and Ru-based electrocatalysts, the peak of the "volcano figure." Ru-based electrocatalysts, on the other hand, are prone to disintegration when exposed to high-acid

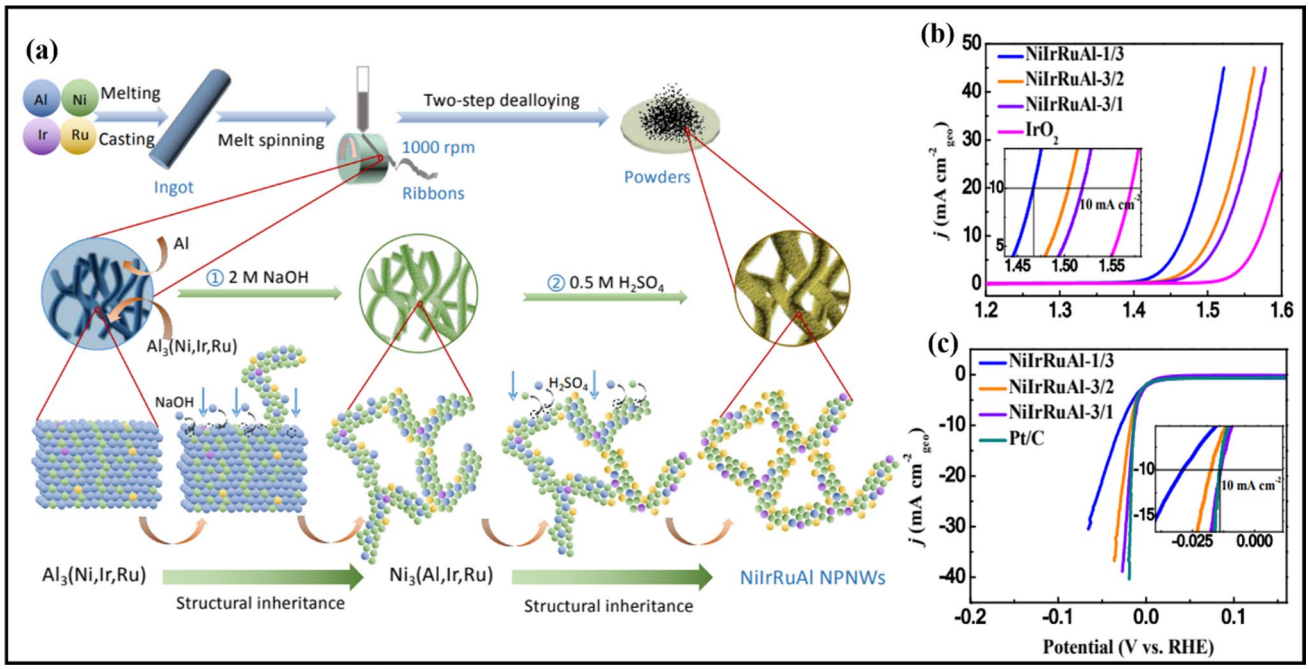

Fig. 7 **a–c** Schematic illustration showing the fabrication process of NiIrRuAl NPNWs [151] reproduced with permission from ref.154, copyright 2020, Journal of Materials Chemistry A

Table 6 Summary of HER and OER performances of inter-noble metal–based electrocatalysts

Catalyst	Overpotential (mV)		Cell voltage (V)	Tafel slope ($mVdec^{-1}$)		Stability	Ref.
	HER	OER		HER	OER		
$Pt_{62}Co_{23}/Ir_{15}$FBNWs	20	300	1.53	–	–	10 h	[152]
SS Pt-RuO_2 HNSs	26	228	–	17	51	100 h	[150]
$Pt_{0.1}La_{0.1}$-IrO_2@NC	–	205	–	–	–	135 h	[153]
PdCu/Ir	21	283	1.51	–	59.6	–	[154]
Rh-Pt-B	31	326	–	32.4	82	–	[155]
IrRh NAs	35	251	1.57	48.4	60.5	20 h	[153]
Ir_{16}–PdCu/C	99	284	1.63	90.3	48	–	[156]
CIS@$Ir_{48}Ru_{52}$ NPs	15.0	244.4	1.47	73.0	–	–	[157]
FeCoNiCuPtIr	21	255	1.51	54.5	61.7	20 h	[158]
NiIrRuAl	14	237	1.464	–	50	10 h	[151]

electrolytes. N. Liu et al. synthesized bifunctional electrocatalysts with elevated performance and low precious metal content. By a two-step dealloying procedure, they developed multimetallic nanoporous nanowires (NiIrRuAl) with various compositions. The enhanced water-splitting performance was evident in its overpotential, as NiIrRuAl-1/3 NPNWs in OER needed an overpotential of just 237 mV at 10 mA cm^{-2}. In contrast, the 0.1 M $HClO_4$ solution for HER required a little overpotential of 14 mV. Importantly, a minor cell potential of 1.464 V was sufficient to operate the bifunctional catalyst to generate 10 mA cm^{-2} and showed better stability. Specifically, the enhanced electrocatalytic performance of NiIrRuAl NPNWs was attributed to (i) electrocatalyst alloying with transition metal, (ii) the combined action of ruthenium and iridium, and (iii) the highly ordered nanostructure [151]. In addition, the HER and OER performances of inter-noble metal–based electrocatalysts are given in Table 6.

Summary and future outlook

In electrochemical water splitting, noble metal–based hybrid materials exhibit outstanding electrocatalytic efficacy because of their inherent high activity, mechanical stability, and more readily accessible surface-active sites. This paper systematically summarizes recent advances in developing electrocatalysts for water splitting based on precious metals. Structure engineering tactics such as adding heteroatoms, defect and strain engineering, single-atom manipulation, and morphology manipulation have all been shown to improve electrocatalytic performance. Overpotentials as low as 2 mV and their rational cause are explained in this article. It has been thoroughly researched that increased surface-active site exposure, synergetic effect, oxygen vacancy, coupling effect, distinct electronic interaction, and string effects are essential for improved electrocatalytic performance in water electrolysis. Despite these significant efforts to improve the composition and morphology of noble metal hybrids, there is still much work to be done before they can be utilized on a wide scale for electrolytic cells, and some outstanding difficulties with noble metal–based hybrids should not be neglected. Given noble metals' high cost and low natural abundance, limiting their consumption is eagerly anticipated. Due to their high price and limited availability of noble metals, minimizing their consumption is eagerly anticipated. Because of their high atom usage and excellent electrocatalytic activity, single-atom catalysts are gaining popularity in electrocatalysis. However, due to the high surface energy, increasing the loading of single atoms will certainly result in significant accumulation and limit the catalytic activity. More efficient ways to increase noble metal usage are desperately needed in the near future. In addition, the synthesis of alloys based on noble metals is substantially more complicated and complex, and several bimetallic structures transform in the reaction. As a result, determining the atomic positioning of these alloys is crucial. In addition, diffusion and segregation of metals can occur under reaction conditions due to interface engineering efforts, particularly during long-standing durability tests. Therefore, additional theoretical and experimental research is required in noble metal–based materials in water-splitting applications.

Author contribution UA. Writing the manuscript, DP. Writing the manuscript, RS. Editing the manuscript and AS. and YC. Supervision, Editing and Reviewing the manuscript.

Funding AS gratefully acknowledges the UGC, New Delhi for their financial support under the BSR Mid-Career Award Scheme (No. F.19-214/2018).

Data availability Not applicable.

Declarations

Ethical approval declaration Not applicable.

Conflict of interest The authors declare no competing interests.

References

1. Li XP, Huang C, Han WK, Ouyang T, Liu ZQ (2021) Transition metal-based electrocatalysts for overall water splitting. Chin Chem Lett 32:2597–2616. https://doi.org/10.1016/j.cclet.2021.01.047
2. Hou Y, Zhuang X, Feng X (2017) Recent advances in Earth-abundant heterogeneous electrocatalysts for photoelectrochemical water splitting. Small Methods 1:1700090. https://doi.org/10.1002/smtd.201700090
3. Zou X, Zhang Y (2015) Noble metal-free hydrogen evolution catalysts for water splitting. Chem Soc Rev 44:5148–5180. https://doi.org/10.1039/c4cs00448e
4. Dresselhaus MS, Thomas IL (2001) Alternative energy technologies. dresselhaus2001. Nature 414:332–337
5. De Luna P, Hahn C, Higgins D, Jaffer SA, Jaramillo TF, Sargent EH (2019) What would it take for renewably powered electrosynthesis to displace petrochemical processes? Science (80) 364. https://doi.org/10.1126/science.aav3506
6. Zhao P, Huang Y, Chen J, Shao S, Miao H, Xia J, Jia C, Hua M (2020) Preparation of meso-tetraphenyl porphyrin modified defect-rich BiOCl with enhanced visible-light photocatalytic activity for antibiotic degradation and mechanism insight. J Photochem Photobiol 3–4:100014. https://doi.org/10.1016/j.jpap.2020.100014
7. Wen J, Ling L, Chen Y, Bian Z (2020) Pyroelectricity effect on photoactivating palladium nanoparticles in PbTiO3 for Suzuki coupling reaction. Chin J Catal 41:1674–1681. https://doi.org/10.1016/S1872-2067(20)63581-1
8. Dong J, Zhang Y, Hussain MI, Zhou W, Chen Y, Wang LN (2022) G-c3 n4: Properties, pore modifications, and photocatalytic applications. Nanomaterials 12:1–35. https://doi.org/10.3390/nano12010121
9. Xu YF, Rao HS, Chen BX, Lin Y, Chen HY, Kuang D, Bin; Su, C.Y. (2015) Achieving highly efficient photoelectrochemical water oxidation with a TiCl4 treated 3D antimony-doped SnO2 macropore/branched α-Fe2O3 nanorod heterojunction photoanode. Adv Sci 2. https://doi.org/10.1002/advs.201500049
10. Tang H, Hessel CM, Wang J, Yang N, Yu R, Zhao H, Wang D (2014) Two-dimensional carbon leading to new photoconversion processes. Chem Soc Rev 43:4281–4299. https://doi.org/10.1039/c3cs60437c
11. Luo J, Im JH, Mayer MT, Schreier M, Nazeeruddin MK, Park NG, Tilley SD, Fan HJ, Grätzel M (2014) Water photolysis at 12.3% efficiency via perovskite photovoltaics and Earth-abundant catalysts. Science (80-) 345:1593–1596. https://doi.org/10.1126/science.1258307
12. Zhou F, Zhou Y, Liu GG, Wang CT, Wang J (2021) Recent advances in nanostructured electrocatalysts for hydrogen evolution reaction. Rare Metals 40:3375–3405. https://doi.org/10.1007/s12598-021-01735-y
13. Liu Y, Chen N, Li W, Sun M, Wu T, Huang B, Yong X, Zhang Q, Gu L, Song H et al (2022) Engineering the synergistic effect of carbon dots-stabilized atomic and subnanometric ruthenium as highly efficient electrocatalysts for robust hydrogen evolution. SmartMat 3:249–259. https://doi.org/10.1002/smm2.1067
14. Yuan J, Cheng X, Wang H, Lei C, Pardiwala S, Yang B, Li Z, Zhang Q, Lei L, Wang S et al (2020) A superaerophobic bimetallic selenides heterostructure for efficient industrial-level oxygen evolution at ultra-high current densities. Nano-Micro Lett 12. https://doi.org/10.1007/s40820-020-00442-0
15. Niu S, Jiang WJ, Wei Z, Tang T, Ma J, Hu JS, Wan LJ (2019) Se-doping activates FeOOH for cost-effective and efficient electrochemical water oxidation. J Am Chem Soc 141:7005–7013. https://doi.org/10.1021/jacs.9b01214
16. Chen G, Zhu Y, Chen HM, Hu Z, Hung SF, Ma N, Dai J, Lin HJ, Chen CT, Zhou W et al (2019) An amorphous nickel–iron-based electrocatalyst with unusual local structures for ultrafast oxygen evolution reaction. Adv Mater 31:1–7. https://doi.org/10.1002/adma.201900883
17. Wang C, Shang H, Xu H, Du Y (2021) Nanoboxes endow non-noble-metal-based electrocatalysts with high efficiency for overall water splitting. J Mater Chem A 9:857–874. https://doi.org/10.1039/d0ta10596a
18. Jo YK, Lee JM, Son S, Hwang SJ (2019) 2D inorganic nanosheet-based hybrid photocatalysts: design, applications, and perspectives. J Photochem Photobiol C: Photochem Rev 40:150–190. https://doi.org/10.1016/j.jphotochemrev.2018.03.002
19. Li W, Cheng G, Sun M, Wu Z, Liu G, Su D, Lan B, Mai S, Chen L, Yu L (2019) C-CoP hollow microporous nanocages based on phosphating regulation: a high-performance bifunctional electrocatalyst for overall water splitting. Nanoscale 11:17084–17092. https://doi.org/10.1039/c9nr05061b
20. Paul R, Zhu L, Chen H, Qu J, Dai L (2019) Recent advances in carbon-based metal-free electrocatalysts. Adv Mater 31:1–24. https://doi.org/10.1002/adma.201806403
21. Kumar R, Ahmed Z, Rai R, Gaur A, Kumari S, Maruyama T, Bagchi V (2019) Uniformly decorated molybdenum carbide/nitride nanostructures on biomass templates for hydrogen evolution reaction applications. ACS Omega 4:14155–14161. https://doi.org/10.1021/acsomega.9b02321
22. Sheng M, Jiang B, Wu B, Liao F, Fan X, Lin H, Li Y, Lifshitz Y, Lee ST, Shao M (2019) Approaching the volcano top: iridium/silicon nanocomposites as efficient electrocatalysts for the hydrogen evolution reaction. ACS Nano 13:2786–2794. https://doi.org/10.1021/acsnano.8b07572
23. Ruqia B, Choi S (2018) Il Pt and Pt–Ni(OH)2 Electrodes for the hydrogen evolution reaction in alkaline electrolytes and their nanoscaled electrocatalysts. ChemSusChem 11:2643–2653. https://doi.org/10.1002/cssc.201800781
24. Danilovic N, Subbaraman R, Strmcnik D, Stamenkovic VR, Markovic NM (2013) Electrocatalysis of the HER in acid and alkaline media. J Serbian Chem Soc 78:2007–2015. https://doi.org/10.2298/JSC131118136D
25. Mahmood N, Yao Y, Zhang JW, Pan L, Zhang X, Zou JJ (2018) Electrocatalysts for hydrogen evolution in alkaline electrolytes: mechanisms, challenges, and prospective solutions. Adv Sci 5. https://doi.org/10.1002/advs.201700464
26. Strmcnik D, Lopes PP, Genorio B, Stamenkovic VR, Markovic NM (2016) Design principles for hydrogen evolution reaction catalyst materials. Nano Energy 29:29–36. https://doi.org/10.1016/j.nanoen.2016.04.017
27. Li M, Duanmu K, Wan C, Cheng T, Zhang L, Dai S, Chen W, Zhao Z, Li P, Fei H et al (2019) Single-atom tailoring of platinum nanocatalysts for high-performance multifunctional electrocatalysis. Nat Catal 2:495–503. https://doi.org/10.1038/s41929-019-0279-6
28. Xu H, Shang H, Wang C, Du Y (2020) Surface and interface engineering of noble-metal-free electrocatalysts for efficient overall water splitting. Coord Chem Rev 418:213374. https://doi.org/10.1016/j.ccr.2020.213374

29. Zahra R, Pervaiz E, Yang M, Rabi O, Saleem Z, Ali M, Farrukh S (2020) A review on nickel cobalt sulphide and their hybrids: Earth abundant, pH stable electro-catalyst for hydrogen evolution reaction. Int J Hydrog Energy 45:24518–24543. https://doi.org/10.1016/j.ijhydene.2020.06.236
30. Yan Y, Xia BY, Zhao B, Wang X (2016) A review on noble-metal-free bifunctional heterogeneous catalysts for overall electrochemical water splitting. J Mater Chem A 4:17587–17603. https://doi.org/10.1039/C6TA08075H
31. Chemistry A European J, 2020, Yu - Earth-abundant transition-metal-based bifunctional electrocatalysts for overall water.pdf.
32. Wang S, Lu A, Zhong CJ (2021) Hydrogen production from water electrolysis: role of catalysts. Nano Converg 8. https://doi.org/10.1186/s40580-021-00254-x
33. Xu Y, Chai X, Liu M, Ren T, Yu S, Wang Z, Li X, Wang L, Wang H (2020) Two-dimensional NiIr@N-doped carbon nanocomposites supported on Ni foam for electrocatalytic overall water splitting. Chem - A Eur J 26:14496–14501. https://doi.org/10.1002/chem.202003473
34. Zhang L, Jang H, Li Z, Liu H, Kim MG, Liu X, Cho J (2021) SrIrO3 modified with laminar Sr2IrO4 as a robust bifunctional electrocatalyst for overall water splitting in acidic media. Chem Eng J 419:129604. https://doi.org/10.1016/j.cej.2021.129604
35. Tahir M, Pan L, Idrees F, Zhang X, Wang L, Zou JJ, Wang ZL (2017) Electrocatalytic oxygen evolution reaction for energy conversion and storage: a comprehensive review. Nano Energy 37:136–157. https://doi.org/10.1016/j.nanoen.2017.05.022
36. Shinagawa T, Garcia-Esparza AT, Takanabe K (2015) Insight on Tafel slopes from a microkinetic analysis of aqueous electrocatalysis for energy conversion. Sci Rep 5. https://doi.org/10.1038/srep13801
37. Wang M, Zhang L, He Y, Zhu H (2021) Recent advances in transition-metal-sulfide-based bifunctional electrocatalysts for overall water splitting. J Mater Chem A 9:5320–5363. https://doi.org/10.1039/d0ta12152e
38. Zhang S, Zhang X, Shi X, Zhou F, Wang R, Li X (2020) Facile fabrication of ultrafine nickel-iridium alloy nanoparticles/graphene hybrid with enhanced mass activity and stability for overall water splitting. J Energy Chem 49:166–173. https://doi.org/10.1016/j.jechem.2020.02.022
39. Sun H, Zhang W, Li JG, Li Z, Ao X, Xue KH, Ostrikov KK, Tang J, Wang C (2021) Rh-engineered ultrathin NiFe-LDH nanosheets enable highly-efficient overall water splitting and urea electrolysis. Appl Catal B Environ 284:119740. https://doi.org/10.1016/j.apcatb.2020.119740
40. Kozuch S, Martin JML (2012) "Turning over" definitions in catalytic cycles. ACS Catal 2:2787–2794. https://doi.org/10.1021/cs3005264
41. Liu H, Yan Z, Chen X, Li J, Zhang L, Liu F, Fan G, Cheng F (2020) Electrodeposition of Pt-decorated Ni(OH) 2 /CeO 2 hybrid as superior bifunctional electrocatalyst for water splitting. Research 2020:1–11. https://doi.org/10.34133/2020/9068270
42. Advanced Materials, 2018, Zhu - Atomic-scale core shell structure engineering induces precise tensile strain to boost.pdf.
43. Wang HF, Tang C, Zhang Q (2018) A review of precious-metal-free bifunctional oxygen electrocatalysts: rational design and applications in Zn−Air batteries. Adv Funct Mater 28. https://doi.org/10.1002/adfm.201803329
44. Wang X, Kolen'Ko YV, Bao XQ, Kovnir K, Liu L (2015) One-step synthesis of self-supported nickel phosphide nanosheet array cathodes for efficient electrocatalytic hydrogen generation. Angew Chem Int Ed 54:8188–8192. https://doi.org/10.1002/anie.201502577
45. Das D, Nanda KK (2016) One-step, integrated fabrication of Co2P nanoparticles encapsulated N, P dual-doped CNTs for highly advanced total water splitting. Nano Energy 30:303–311. https://doi.org/10.1016/j.nanoen.2016.10.024
46. Chen X, Li D, Li Y, Zhan W, Huang C, Chen R, Wang W, Ni H, Chu PK (2022) Short-brush NiFeOxHy films and the Pt derivative as high-performance electrode materials for efficient electrocatalytic water splitting. Appl Surf Sci 574:151636. https://doi.org/10.1016/j.apsusc.2021.151636
47. Diaz-Morales O, Raaijman S, Kortlever R, Kooyman PJ, Wezendonk T, Gascon J, Fu WT, Koper MTM (2016) Iridium-based double perovskites for efficient water oxidation in acid media. Nat Commun 7. https://doi.org/10.1038/ncomms12363
48. Rao RR, Kolb MJ, Halck NB, Pedersen AF, Mehta A, You H, Stoerzinger KA, Feng Z, Hansen HA, Zhou H et al (2017) Towards identifying the active sites on RuO2(110) in catalyzing oxygen evolution. Energy Environ Sci 10:2626–2637. https://doi.org/10.1039/c7ee02307c
49. Zhang X, Zhao Y, Zhao Y, Shi R, Waterhouse GIN, Zhang T (2019) A simple synthetic strategy toward defect-rich porous monolayer NiFe-layered double hydroxide nanosheets for efficient electrocatalytic water oxidation. Adv Energy Mater 9:1–7. https://doi.org/10.1002/aenm.201900881
50. Yin S, Tu W, Sheng Y, Du Y, Kraft M, Borgna A, Xu R (2018) A highly efficient oxygen evolution catalyst consisting of interconnected nickel–iron-layered double hydroxide and carbon nanodomains. Adv Mater 30:1–9. https://doi.org/10.1002/adma.201705106
51. Chen Z, Liu D, Gao Y, Zhao Y, Xiao W, Xu G, Ma T, Wu Z, Wang L (2022) Corrosive-coordinate engineering to construct 2D-3D nanostructure with trace Pt as efficient bifunctional electrocatalyst for overall water splitting. Sci China Mater 65:1217–1224. https://doi.org/10.1007/s40843-021-1943-5
52. Yu J, Wang Q, O'Hare D, Sun L (2017) Preparation of two dimensional layered double hydroxide nanosheets and their applications. Chem Soc Rev 46:5950–5974. https://doi.org/10.1039/c7cs00318h
53. Pavel OD, Zăvoianu R, Angelescu E (2016) The effect of modifying cations on the catalytic activity of hydrotalcite-like compounds in 1, 4-addition reactions. Rev Roum Chim 61:671–681
54. Long X, Wang Z, Xiao S, An Y, Yang S (2016) Transition metal based layered double hydroxides tailored for energy conversion and storage. Mater Today 19:213–226. https://doi.org/10.1016/j.mattod.2015.10.006
55. Wang Z, Long X, Yang S (2018) Effects of metal combinations on the electrocatalytic properties of transition-metal-based layered double hydroxides for water oxidation: a perspective with insights. ACS Omega 3:16529–16541. https://doi.org/10.1021/acsomega.8b02565
56. Luis, F.; Moncayo, G. No 主観的健康感を中心とした在宅高齢者における 健康関連指標に関する共分散構造分析Title.
57. Feng Y, Li Z, Li S, Yang M, Ma R, Wang J (2022) One stone two birds: vanadium doping as dual roles in self-reduced Pt clusters and accelerated water splitting. J Energy Chem 66:493–501. https://doi.org/10.1016/j.jechem.2021.08.061
58. Yin D, Cao YD, Chai DF, Fan LL, Gao GG, Wang ML, Liu H, Kang Z (2022) A WOx mediated interface boosts the activity and stability of Pt-catalyst for alkaline water splitting. Chem Eng J 431:133287. https://doi.org/10.1016/j.cej.2021.133287
59. Tran DT, Le HT, Luyen Doan TL, Kim NH, Lee JH (2019) Pt nanodots monolayer modified mesoporous Cu@Cu x O nanowires for improved overall water splitting reactivity. Nano Energy 59:216–228. https://doi.org/10.1016/j.nanoen.2019.02.050
60. Yu X, Guo J, Li B, Xu J, Gao P, Hui KS, Hui KN, Shao H (2021) Sub-nanometer Pt clusters on defective NiFe LDH nanosheets as trifunctional electrocatalysts for water splitting and rechargeable hybrid sodium-air batteries. ACS Appl Mater Interfaces 13:26891–26903. https://doi.org/10.1021/acsami.1c03337

61. Anantharaj S, Karthick K, Venkatesh M, Simha TVSV, Salunke AS, Ma L, Liang H, Kundu S (2017) Enhancing electrocatalytic total water splitting at few layer Pt-NiFe layered double hydroxide interfaces. Nano Energy 39:30–43. https://doi.org/10.1016/j.nanoen.2017.06.027
62. Jeong S, Mai HD, Nam KH, Park CM, Jeon KJ (2022) Self-healing graphene-templated platinum-nickel oxide heterostructures for overall water splitting. ACS Nano 16:930–938. https://doi.org/10.1021/acsnano.1c08506
63. Yan Q, Yan P, Wei T, Wang G, Cheng K, Ye K, Zhu K, Yan J, Cao D, Li Y (2019) A highly efficient and durable water splitting system: platinum sub-nanocluster functionalized nickel-iron layered double hydroxide as the cathode and hierarchical nickel-iron selenide as the anode. J Mater Chem A 7:2831–2837. https://doi.org/10.1039/c8ta10789k
64. Zheng X, Cao Y, Han X, Liu H, Wang J, Zhang Z, Wu X, Zhong C, Hu W, Deng Y (2019) Pt embedded Ni3Se2@NiOOH core-shell dendrite-like nanoarrays on nickel as bifunctional electrocatalysts for overall water splitting. Sci China Mater 62:1096–1104. https://doi.org/10.1007/s40843-019-9413-5
65. Fu M, Zhang Q, Sun Y, Ning G, Fan X, Wang H, Lu H, Zhang Y, Wang H (2020) Ni–Fe nanocubes embedded with Pt nanoparticles for hydrogen and oxygen evolution reactions. Int J Hydrog Energy 45:20832–20842. https://doi.org/10.1016/j.ijhydene.2020.05.170
66. Li C, Xu Y, Yang D, Qian X, Chai X, Wang Z, Li X, Wang L, Wang H (2019) Boosting electrocatalytic activities of Pt-based mesoporous nanoparticles for overall water splitting by a facile Ni, P co-incorporation strategy. ACS Sustain Chem Eng 7:9709–9716. https://doi.org/10.1021/acssuschemeng.9b01484
67. Guan Y, Liu Y (2021) Pt modified Ni-Mo-based hydrates as bifunctional electrocatalysts for overall water splitting. New J Chem 45:16313–16318. https://doi.org/10.1039/d1nj02046c
68. Xu W, Chang J, Cheng Y, Liu H, Li J, Ai Y, Hu Z, Zhang X, Wang Y, Liang Q et al (2022) A multi-step induced strategy to fabricate core-shell Pt-Ni alloy as symmetric electrocatalysts for overall water splitting. Nano Res 15:965–971. https://doi.org/10.1007/s12274-021-3582-x
69. Zhao Y, Gao Y, Chen Z, Li Z, Ma T, Wu Z, Wang L (2021) Trifle Pt coupled with NiFe hydroxide synthesized via corrosion engineering to boost the cleavage of water molecule for alkaline water-splitting. Appl Catal B Environ 297:120395. https://doi.org/10.1016/j.apcatb.2021.120395
70. Ye B, Jiang R, Yu Z, Hou Y, Huang J, Zhang B, Huang Y, Zhang Y, Zhang R (2019) Pt (1 1 1) quantum dot engineered Fe-MOF nanosheet arrays with porous core-shell as an electrocatalyst for efficient overall water splitting. J Catal 380:307–317. https://doi.org/10.1016/j.jcat.2019.09.038
71. Zhang H, Liu Y, Wu H, Zhou W, Kou Z, Pennycook SJ, Xie J, Guan C, Wang J (2018) Open hollow Co-Pt clusters embedded in carbon nanoflake arrays for highly efficient alkaline water splitting. J Mater Chem A 6:20214–20223. https://doi.org/10.1039/c8ta07101b
72. Chen J, Wang J, Chen J, Wang L (2017) A bifunctional electrocatalyst of PtNi nanoparticles immobilized on three-dimensional carbon nanofiber mats for efficient and stable water splitting in both acid and basic media. J Mater Sci 52:13064–13077. https://doi.org/10.1007/s10853-017-1410-1
73. Lu S, Zhu K, Fan D, Hu X (2022) A novel PdC monolayer with fully dispersed Pd atoms and a rigid carbon backbone: an intrinsic versatile electrocatalyst for overall water splitting and the corresponding reverse reaction. Phys Chem Chem Phys 24:6811–6819. https://doi.org/10.1039/d1cp05392b
74. Electroanalysis, 2020, Ipadeola - Bifunctional behavior of Pd Ni nanocatalysts on MOF-derived carbons for alkaline (1).pdf.
75. Ipadeola AK, Ozoemena KI (2020) Alkaline water-splitting reactions over Pd/Co-MOF-derived carbon obtainedviamicrowave-assisted synthesis. RSC Adv 10:17359–17368. https://doi.org/10.1039/d0ra02307h
76. Zhang H, Jiang Q, Hadden JHL, Xie F, Riley DJ (2021) Pd ion-exchange and ammonia etching of a Prussian blue analogue to produce a high-performance water-splitting catalyst. Adv Funct Mater 31. https://doi.org/10.1002/adfm.202008989
77. Karuppasamy L, Gurusamy L, Anandan S, Liu CH, Wu JJ (2022) Defect-enriched heterointerfaces N–MoO2–Mo2C supported Pd nanocomposite as a novel multifunctional electrocatalyst for oxygen reduction reaction and overall water splitting. Mater Today Chem 24. https://doi.org/10.1016/j.mtchem.2022.100799
78. Zhang W, Jiang X, Dong Z, Wang J, Zhang N, Liu J, Xu GR, Wang L (2021) Porous Pd/NiFeOx nanosheets enhance the pH-universal overall water splitting. Adv Funct Mater 31:1–11. https://doi.org/10.1002/adfm.202107181
79. Luo F, Zhang Q, Yu X, Xiao S, Ling Y, Hu H, Guo L, Yang Z, Huang L, Cai W et al (2018) Palladium phosphide as a stable and efficient electrocatalyst for overall water splitting. Angew Chem Int Ed 57:14862–14867. https://doi.org/10.1002/anie.201810102
80. Butenko DS, Li S, Kotsyubynsky VO, Boychuk VM, Dubinko VI, Kolkovsky PI, Liedienov NA, Klyui NI, Han W, Zatovsky IV (2021) Palladium nanoparticles embedded in microporous carbon as electrocatalysts for water splitting in alkaline media. Int J Hydrog Energy 46:21462–21474. https://doi.org/10.1016/j.ijhydene.2021.03.242
81. Qin Q, Jang H, Chen L, Li P, Wei T, Liu X, Cho J (2019) Coupling a low loading of IrP 2 , PtP 2 , or Pd 3 P with heteroatom-doped nanocarbon for overall water-splitting cells and zinc-air batteries. ACS Appl Mater Interfaces 11:16461–16473. https://doi.org/10.1021/acsami.8b21155
82. Pandey A, Mukherjee A, Chakrabarty S, Chanda D, Basu S (2019) Interface engineering of an RGO/MoS2/Pd 2D heterostructure for electrocatalytic overall water splitting in alkaline medium. ACS Appl Mater Interfaces 11:42094–42103. https://doi.org/10.1021/acsami.9b13358
83. Guo J, Sun J, Sun Y, Liu Q, Zhang X (2019) Electrodepositing Pd on NiFe layered double hydroxide for improved water electrolysis. Mater Chem Front 3:842–850. https://doi.org/10.1039/c9qm00052f
84. Kaushik P, Kaur G, Ram Chaudhary G, Batra U (2021) Cleaner way for overall water splitting reaction by using palladium and cobalt based nanocomposites prepared from mixed metallosurfactants. Appl Surf Sci 556:149769. https://doi.org/10.1016/j.apsusc.2021.149769
85. Duan, H.; Li, D.; Tang, Y.; He, Y.; Wang, R.; Lv, H.; Lopes, P.P.; Paulikas, A.P.; Li, H.; Mao, S.X.; et al. 4-Duan2017.Pdf. 2017.
86. Qin Q, Jang H, Chen L, Nam G, Liu X, Cho J (2018) Low loading of RhxP and RuP on N, P codoped carbon as two trifunctional electrocatalysts for the oxygen and hydrogen electrode reactions. Adv Energy Mater 8:1–12. https://doi.org/10.1002/aenm.201801478
87. Cao D, Xu H, Cheng D (2020) Construction of defect-rich RhCu nanotubes with highly active Rh3Cu1 alloy phase for overall water splitting in all pH values. Adv Energy Mater 10:1–12. https://doi.org/10.1002/aenm.201903038
88. Wu X, Wang R, Li W, Feng B, Hu W (2021) Rh2P nanoparticles partially embedded in N/P-doped carbon scaffold at ultralow metal loading for high current density water electrolysis. ACS Appl Nano Mater 4:2–9. https://doi.org/10.1021/acsanm.0c03126
89. Narwade SS, Mali SM, Sapner VS, Sathe BR (2020) Graphene oxide decorated with Rh nanospheres for electrocatalytic water splitting. ACS Appl Nano Mater 3:12288–12296. https://doi.org/10.1021/acsanm.0c02762

90. Zhao J, Zhang W, Zhang J, Chen X, Wu Y, Li C, Zhang X, Yang F (2020) The electropositive environment of Rh in Rh1Sn2/SWNTs for boosting trifunctional electrocatalysis. Int J Hydrog Energy 45:32050–32058. https://doi.org/10.1016/j.ijhydene.2020.08.283
91. Zhang W, Zhao J, Zhang J, Chen X, Zhang X, Yang F (2020) Electronic asymmetric distribution of RhCu bimetallic nanocrystals for enhancing trifunctional electrocatalysis. ACS Appl Mater Interfaces 12:10299–10306. https://doi.org/10.1021/acsami.9b19980
92. Zhang B, Zhu C, Wu Z, Stavitski E, Lui YH, Kim TH, Liu H, Huang L, Luan X, Zhou L et al (2020) Integrating Rh species with NiFe-layered double hydroxide for overall water splitting. Nano Lett 20:136–144. https://doi.org/10.1021/acs.nanolett.9b03460
93. Zhu K, Chen J, Wang W, Liao J, Dong J, Chee MOL, Wang N, Dong P, Ajayan PM, Gao S et al (2020) Etching-doping sedimentation equilibrium strategy: accelerating kinetics on hollow Rh-doped CoFe-layered double hydroxides for water splitting. Adv Funct Mater 30:1–10. https://doi.org/10.1002/adfm.202003556
94. Jiang X, Dong Z, Wang J, Zhang N, Xu GR, Zhang W, Lai J, Li Z, Wang L (2021) Self-assembly of functionalized Echinops-like Rh porous nanostructure electrocatalysts for highly efficient seawater splitting. J Mater Chem C 9:8314–8322. https://doi.org/10.1039/d1tc01722e
95. Chen MT, Duan JJ, Feng JJ, Mei LP, Jiao Y, Zhang L, Wang AJ (2022) Iron, rhodium-codoped Ni2P nanosheets arrays supported on nickel foam as an efficient bifunctional electrocatalyst for overall water splitting. J Colloid Interface Sci 605:888–896. https://doi.org/10.1016/j.jcis.2021.07.101
96. Fan R, Mu Q, Wei Z, Peng Y, Shen M (2020) Atomic Ir-doped NiCo layered double hydroxide as a bifunctional electrocatalyst for highly efficient and durable water splitting. J Mater Chem A 8:9871–9881. https://doi.org/10.1039/d0ta03272g
97. Gao W, Xu Q, Wang Z, Wang M, Ren X, Yuan G, Wang Q (2020) Self-assembly of homointerface engineered IrCo0.14 bracelet-like nanorings as efficient and stable bifunctional catalysts for electrochemical water splitting in acidic media. Electrochim Acta 337:135738. https://doi.org/10.1016/j.electacta.2020.135738
98. Chen J, Wang Y, Qian G, Yu T, Wang Z, Luo L, Shen F, Yin S (2021) In situ growth of volcano-like FeIr alloy on nickel foam as efficient bifunctional catalyst for overall water splitting at high current density. Chem Eng J 421:129892. https://doi.org/10.1016/j.cej.2021.129892
99. Feng Q, Wang Q, Zhang Z, Xiong Y, Li H, Yao Y, Yuan XZ, Williams MC, Gu M, Chen H et al (2019) Highly active and stable ruthenate pyrochlore for enhanced oxygen evolution reaction in acidic medium electrolysis. Appl Catal B Environ 244:494–501. https://doi.org/10.1016/j.apcatb.2018.11.071
100. Wang W, Kuai L, Cao W, Huttula M, Ollikkala S, Ahopelto T, Honkanen AP, Huotari S, Yu M, Geng B (2017) Mass-production of mesoporous MnCo2O4 spinels with manganese(IV)- and cobalt(II)-rich surfaces for superior bifunctional oxygen electrocatalysis. Angew Chem Int Ed 56:14977–14981. https://doi.org/10.1002/anie.201708765
101. Zhang G, Lan ZA, Lin L, Lin S, Wang X (2016) Overall water splitting by Pt/g-C3N4 photocatalysts without using sacrificial agents. Chem Sci 7:3062–3066. https://doi.org/10.1039/c5sc04572j
102. Yang L, Chen H, Shi L, Li X, Chu X, Chen W, Li N, Zou X (2019) Enhanced iridium mass activity of 6H-phase, Ir-based perovskite with nonprecious incorporation for acidic oxygen evolution electrocatalysis. ACS Appl Mater Interfaces 11:42006–42013. https://doi.org/10.1021/acsami.9b11287
103. Tsai H, Nie W, Blancon JC, Stoumpos CC, Asadpour R, Harutyunyan B, Neukirch AJ, Verduzco R, Crochet JJ, Tretiak S et al (2016) High-efficiency two-dimensional ruddlesden-popper perovskite solar cells. Nature 536:312–317. https://doi.org/10.1038/nature18306
104. Fu L, Hu X, Li Y, Cheng G, Luo W (2019) IrW nanobranches as an advanced electrocatalyst for pH-universal overall water splitting. Nanoscale 11:8898–8905. https://doi.org/10.1039/c9nr01690b
105. Wu W, Liu J, Johannes N (2021) Electrodeposition of Ir–Co thin films on copper foam as high-performance electrocatalysts for efficient water splitting in alkaline medium. Int J Hydrog Energy 46:609–621. https://doi.org/10.1016/j.ijhydene.2020.09.268
106. Zhang J, Wang G, Liao Z, Zhang P, Wang F, Zhuang X, Zschech E, Feng X (2017) Iridium nanoparticles anchored on 3D graphite foam as a bifunctional electrocatalyst for excellent overall water splitting in acidic solution. Nano Energy 40:27–33. https://doi.org/10.1016/j.nanoen.2017.07.054
107. Xie Y, Long X, Li X, Chang C, Qu K, Yang Z (2021) The template synthesis of ultrathin metallic Ir nanosheets as a robust electrocatalyst for acidic water splitting. Chem Commun 57:8620–8623. https://doi.org/10.1039/d1cc02349g
108. Pedireddy S, Jimenez-Sandoval R, Ravva MK, Nayak C, Anjum DH, Jha SN, Katuri KP, Saikaly PE (2021) Harnessing the extracellular electron transfer capability of geobacter sulfurreducens for ambient synthesis of stable bifunctional single-atom electrocatalyst for water splitting. Adv Funct Mater 31:1–10. https://doi.org/10.1002/adfm.202010916
109. Luo F, Guo L, Xie Y, Xu J, Qu K, Yang Z (2020) Iridium nanorods as a robust and stable bifunctional electrocatalyst for pH-universal water splitting. Appl Catal B Environ 279:119394. https://doi.org/10.1016/j.apcatb.2020.119394
110. Ren Z, Jin L, Deng L, Ming R, Zhang A, Zhou X, Chai B, Zhu Y (2019) A silicon-doped iridium electrode prepared by magnetron-sputtering as an advanced electrocatalyst for overall water splitting in acidic media. Sustain Energy Fuels 3:2321–2328. https://doi.org/10.1039/c9se00250b
111. Wang H, Chen ZN, Wu D, Cao M, Sun F, Zhang H, You H, Zhuang W, Cao R (2021) Significantly enhanced overall water splitting performance by partial oxidation of Ir through Au modification in core-shell alloy structure. J Am Chem Soc 143:4639–4645. https://doi.org/10.1021/jacs.0c12740
112. Kim Y, Yu A, Lee Y (2021) Iridium-cobalt alloy nanotubes as a bifunctional electrocatalyst for pH-universal overall water splitting. Bull Korean Chem Soc 42:1524–1533. https://doi.org/10.1002/bkcs.12382
113. Hu H, Kazim FMD, Ye Z, Xie Y, Zhang Q, Qu K, Xu J, Cai W, Xiao S, Yang Z (2020) Electronically delocalized Ir enables efficient and stable acidic water splitting. J Mater Chem A 8:20168–20174. https://doi.org/10.1039/d0ta07416k
114. Li X, Xue W, Mo R, Yang S, Li H, Zhong J (2019) In situ growth of minimal Ir-incorporated CoxNi1-xO nanowire arrays on Ni foam with improved electrocatalytic activity for overall water splitting. Chin J Catal 40:1576–1584. https://doi.org/10.1016/S1872-2067(19)63414-5
115. Ren Z, Wang Y, Jiang H, Jiang H, Tian M, Liu Y, Han J, Fang H, Zhu Y (2022) A novel bifunctional catalyst for overall water electrolysis: nano Ir: XMn(1- x)oyhybrids with L12-IrMn3phase. Chem Commun 58:685–688. https://doi.org/10.1039/d1cc06062g
116. Zhang Z, Xia Y, Ye M, Wen D, Zhang W, Peng W, Tian L, Hu W (2022) Low Ir-content Ir/Fe@NCNT bifunctional catalyst for efficient water splitting. Int J Hydrog Energy 47:13371–13385. https://doi.org/10.1016/j.ijhydene.2022.02.078
117. Wu X, Feng B, Li W, Niu Y, Yu Y, Lu S, Zhong C, Liu P, Tian Z, Chen L et al (2019) Metal-support interaction boosted

electrocatalysis of ultrasmall iridium nanoparticles supported on nitrogen doped graphene for highly efficient water electrolysis in acidic and alkaline media. Nano Energy 62:117–126. https://doi.org/10.1016/j.nanoen.2019.05.034
118. Yi L, Feng B, Chen N, Li W, Li J, Fang C, Yao Y, Hu W (2021) Electronic interaction boosted electrocatalysis of iridium nanoparticles on nitrogen-doped graphene for efficient overall water splitting in acidic and alkaline media. Chem Eng J 415:129034. https://doi.org/10.1016/j.cej.2021.129034
119. Yao W, Jiang X, Li Y, Zhao C, Ding L, Sun D, Tang Y (2021) N-doped graphene anchored ultrasmall Ir nanoparticles as bifunctional electrocatalyst for overall water splitting. Green. Energy Environ:1–8. https://doi.org/10.1016/j.gee.2021.01.011
120. Luo F, Hu H, Zhao X, Yang Z, Zhang Q, Xu J, Kaneko T, Yoshida Y, Zhu C, Cai W (2020) Robust and stable acidic overall water splitting on Ir single atoms. Nano Lett 20:2120–2128. https://doi.org/10.1021/acs.nanolett.0c00127
121. Huang B, Ma Y, Xiong Z, Xiao Z, Wu P, Jiang P, Liang M (2021) Polyoxometalate-derived Ir/WOx/rGO nanocomposites for enhanced electrocatalytic water splitting. Energy Environ Mater 4:681–686. https://doi.org/10.1002/eem2.12150
122. Reier T, Oezaslan M, Strasser P (2012) Electrocatalytic oxygen evolution reaction (OER) on Ru, Ir, and pt catalysts: a comparative study of nanoparticles and bulk materials. ACS Catal 2:1765–1772. https://doi.org/10.1021/cs3003098
123. Cen J, Shen PK, Zeng Y (2022) Ru doping NiCoP hetero-nanowires with modulated electronic structure for efficient overall water splitting. J Colloid Interface Sci 610:213–220. https://doi.org/10.1016/j.jcis.2021.12.028
124. Maiti A, Srivastava SK (2021) Ru-doped CuO/MoS2nanostructures as bifunctional water-splitting electrocatalysts in alkaline media. ACS Appl Nano Mater 4:7675–7685. https://doi.org/10.1021/acsanm.1c00791
125. Yan S, Liao W, Zhong M, Li W, Wang C, Pinna N, Chen W, Lu X (2022) Partially oxidized ruthenium aerogel as highly active bifunctional electrocatalyst for overall water splitting in both alkaline and acidic media. Appl Catal B Environ 307:121199. https://doi.org/10.1016/j.apcatb.2022.121199
126. Yang B, Du Y, Shao M, Bin D, Zhao Q, Xu Y, Liu B, Lu H (2022) MOF-derived RuCoP nanoparticles-embedded nitrogen-doped polyhedron carbon composite for enhanced water splitting in alkaline media. J Colloid Interface Sci 616:803–812. https://doi.org/10.1016/j.jcis.2022.02.119
127. Cen J, Jiang E, Zhu Y, Chen Z, Tsiakaras P, Shen PK (2021) Enhanced electrocatalytic overall water splitting over novel one-pot synthesized Ru–MoO3-x and Fe3O4–NiFe layered double hydroxide on Ni foam. Renew Energy 177:1346–1355. https://doi.org/10.1016/j.renene.2021.06.005
128. Pei Y, Guo S, Ju Q, Li Z, Zhuang P, Ma R, Hu Y, Zhu Y, Yang M, Zhou Y et al (2020) Interface engineering with ultralow ruthenium loading for efficient water splitting. ACS Appl Mater Interfaces 12:36177–36185. https://doi.org/10.1021/acsami.0c09593
129. Zhang J, Zhao Z, Wang R, Du P, He X, Zhang X, Yang J, Liu W, Huang K, Pan X et al (2021) Molten-salt thermosynthesis of amorphous RuCoFe nanosheets as bifunctional catalysts for electrochemical water splitting. Appl Phys A Mater Sci Process 127:1–7. https://doi.org/10.1007/s00339-021-04756-7
130. Yang K, Xu P, Lin Z, Yang Y, Jiang P, Wang C, Liu S, Gong S, Hu L, Chen Q (2018) Ultrasmall Ru/Cu-doped RuO2 complex embedded in amorphous carbon skeleton as highly active bifunctional electrocatalysts for overall water splitting. Small 14:1–10. https://doi.org/10.1002/smll.201803009
131. Wu D, Chen D, Zhu J, Mu S (2021) Ultralow Ru incorporated amorphous cobalt-based oxides for high-current-density overall water splitting in alkaline and seawater media. Small 17:1–9. https://doi.org/10.1002/smll.202102777
132. Tuo Y, Liu W, Chen C, Lu Q, Zhou Y, Zhang J (2021) Constructing RuCoOx/NC nanosheets with low crystallinity within ZIF-9 as bifunctional catalysts for highly efficient overall water splitting. Chem - An Asian J 16:2511–2519. https://doi.org/10.1002/asia.202100629
133. Liu J, Zheng Y, Jiao Y, Wang Z, Lu Z, Vasileff A, Qiao SZ (2018) NiO as a bifunctional promoter for RuO2 toward superior overall water splitting. Small 14:1–10. https://doi.org/10.1002/smll.201704073
134. Fan Z, Jiang J, Ai L, Shao Z, Liu S (2019) Rational design of ruthenium and cobalt-based composites with rich metal-insulator interfaces for efficient and stable overall water splitting in acidic electrolyte. ACS Appl Mater Interfaces 11:47894–47903. https://doi.org/10.1021/acsami.9b15844
135. Yao Q, Huang B, Zhang N, Sun M, Shao Q, Huang X (2019) Channel-rich RuCu nanosheets for pH-universal overall water splitting electrocatalysis. Angew Chem Int Ed 58:13983–13988. https://doi.org/10.1002/anie.201908092
136. Xue Y, Yan Q, Bai X, Xu Y, Zhang X, Li Y, Zhu K, Ye K, Yan J, Cao D et al (2022) Ruthenium-nickel-cobalt alloy nanoparticles embedded in hollow carbon microtubes as a bifunctional mosaic catalyst for overall water splitting. J Colloid Interface Sci 612:710–721. https://doi.org/10.1016/j.jcis.2022.01.001
137. Zhao M, Li H, Li W, Li J, Yi L, Hu W, Li CM (2020) Ru-doping enhanced electrocatalysis of metal–organic framework nanosheets toward overall water splitting. Chem - A Eur J 26:17091–17096. https://doi.org/10.1002/chem.202002072
138. Wang D, Chen Y, Fan L, Xiao T, Meng T, Xing Z, Yang X (2022) Bulk and surface dual modification of nickel-cobalt spinel with ruthenium toward highly efficient overall water splitting. Appl Catal B Environ 305:121081. https://doi.org/10.1016/j.apcatb.2022.121081
139. Wu Y, Yao R, Zhao Q, Li J, Liu G (2022) La-RuO2 nanocrystals with efficient electrocatalytic activity for overall water splitting in acidic media: synergistic effect of La doping and oxygen vacancy. Chem Eng J 439:135699. https://doi.org/10.1016/j.cej.2022.135699
140. Zhang J, Lian J, Jiang Q, Wang G (2022) Boosting the OER/ORR/HER activity of Ru-doped Ni/Co oxides heterostructure. Chem Eng J 439:135634. https://doi.org/10.1016/j.cej.2022.135634
141. Li W, Feng B, Yi L, Li J, Hu W (2021) Highly efficient alkaline water splitting with Ru-doped Co−V layered double hydroxide nanosheets as a bifunctional electrocatalyst. ChemSusChem 14:730–737. https://doi.org/10.1002/cssc.202002509
142. Ye L, Zhang Y, Guo B, Cao D, Gong Y (2021) Ru doping induces the construction of a unique core-shell microflower self-supporting electrocatalyst for highly efficient overall water splitting. Dalton Trans 50:13951–13960. https://doi.org/10.1039/d1dt02341a
143. Liu Z, Zha M, Wang Q, Hu G, Feng L (2020) Overall water-splitting reaction efficiently catalyzed by a novel bi-functional Ru/Ni3N-Ni electrode. Chem Commun 56:2352–2355. https://doi.org/10.1039/c9cc09187d
144. Yang J, Shao Q, Huang B, Sun M, Huang X (2019) pH-universal water splitting catalyst: Ru-Ni nanosheet assemblies. iScience 11:492–504. https://doi.org/10.1016/j.isci.2019.01.004
145. Liu H, Zhang R, Chen L, Wang L, Guo Y, Yang Y (2021) Synergistic coupling of nickel boride with Ru cluster as a highly active multifunctional electrocatalyst for overall water splitting and glucose electrolysis. Adv Sustain Syst 5:1–8. https://doi.org/10.1002/adsu.202000184
146. Ai L, Wang Y, Luo Y, Tian Y, Yang S, Chen M, Jiang J (2022) Robust interfacial Ru-RuO2 heterostructures for highly efficient and ultrastable oxygen evolution reaction and overall water splitting in acidic media. J Alloys Compd 902:163787. https://doi.org/10.1016/j.jallcom.2022.163787

147. Ding J, Shao Q, Feng Y, Huang X (2018) Ruthenium-nickel sandwiched nanoplates for efficient water splitting electrocatalysis. Nano Energy 47:1–7. https://doi.org/10.1016/j.nanoen.2018.02.017
148. Fan Z, Liao F, Shi H, Liu Y, Shao M, Kang Z (2020) Highly efficient water splitting over a RuO2/F-doped graphene electrocatalyst with ultra-low ruthenium content. Inorg Chem Front 7:2188–2194. https://doi.org/10.1039/d0qi00095g
149. Shan J, Guo C, Zhu Y, Chen S, Song L, Jaroniec M, Zheng Y, Qiao SZ (2019) Charge-redistribution-enhanced nanocrystalline Ru@IrOx electrocatalysts for oxygen evolution in acidic media. Chem 5:445–459. https://doi.org/10.1016/j.chempr.2018.11.010
150. Wang J, Yang H, Li F, Li L, Wu J, Liu S, Cheng T, Xu Y, Shao Q, Huang X (2022) Single-site Pt-doped RuO 2 hollow nanospheres with interstitial C for high-performance acidic overall water splitting. Sci Adv 8:1–12. https://doi.org/10.1126/sciadv.abl9271
151. Liu N, Zhang Y, Ma W, Zhang Z, Yin K, Si C, Kou T (2020) Hierarchically porous nickel-iridium-ruthenium-aluminum alloys with tunable compositions and electrocatalytic activities towards the oxygen/hydrogen evolution reaction in acid electrolyte. J Mater Chem A 8:6245–6255. https://doi.org/10.1039/d0ta00445f
152. Sun Y, Huang B, Li Y, Xing Y, Luo M, Li N, Xia Z, Qin Y, Su D, Wang L et al (2019) Trifunctional fishbone-like PtCo/Ir enables high-performance zinc-air batteries to drive the water-splitting catalysis. Chem Mater 31:8136–8144. https://doi.org/10.1021/acs.chemmater.9b02892
153. Hao S, Wang Y, Zheng G, Qiu L, Xu N, He Y, Lei L, Zhang X (2020) Tuning electronic correlations of ultra-small IrO2 nanoparticles with La and Pt for enhanced oxygen evolution performance and long-durable stability in acidic media. Appl Catal B Environ 266:1–8. https://doi.org/10.1016/j.apcatb.2020.118643
154. Li M, Zhao Z, Xia Z, Luo M, Zhang Q, Qin Y, Tao L, Yin K, Chao Y, Gu L et al (2021) Exclusive strain effect boosts overall water splitting in PdCu/Ir core/shell nanocrystals. Angew Chem 133:8324–8331. https://doi.org/10.1002/ange.202016199
155. Wang Y, Guo W, Zhu Z, Xu K, Zhang H, Wei W, Xiao X, Liang W, He M, Yu T et al (2022) Interfacial boron modification on mesoporous octahedral rhodium shell and its enhanced electrocatalysis for water splitting and oxygen reduction. Chem Eng J 435:134982. https://doi.org/10.1016/j.cej.2022.134982
156. Qin Y, Wang Z, Yu W, Sun Y, Wang D, Lai J, Guo S, Wang L (2021) High valence M-incorporated PdCu nanoparticles (M = Ir, Rh, Ru) for water electrolysis in alkaline solution. Nano Lett 21:5774–5781. https://doi.org/10.1021/acs.nanolett.1c01581
157. Joo J, Jin H, Oh A, Kim B, Lee J, Baik H, Joo SH, Lee K (2018) An IrRu alloy nanocactus on Cu2-xS@IrSy as a highly efficient bifunctional electrocatalyst toward overall water splitting in acidic electrolytes. J Mater Chem A 6:16130–16138. https://doi.org/10.1039/c8ta04886j
158. Lu Y, Huang K, Cao X, Zhang L, Wang T, Peng D, Zhang B, Liu Z, Wu J, Zhang Y et al (2022) Atomically dispersed intrinsic hollow sites of M-M1-M (M1 = Pt, Ir; M = Fe, Co, Ni, Cu, Pt, Ir) on FeCoNiCuPtIr nanocrystals enabling rapid water redox. Adv Funct Mater 2110645:1–9. https://doi.org/10.1002/adfm.202110645